

Review

# Metal–Organic Frameworks (MOFs) and Materials Derived from MOFs as Catalysts for the Development of Green Processes

Gonzalo Valdebenito, Marco González-Carvajal, Luis Santibañez and Patricio Cancino \* 

Facultad de Ciencias Químicas y Farmacéuticas, Universidad de Chile, Santiago 8380000, Chile; gonvaldebenito@ug.uchile.cl (G.V.); mgonzalezcar96@gmail.com (M.G.-C.); santibanezcamosl@gmail.com (L.S.)

\* Correspondence: pcancino@ciq.uchile.cl

**Abstract:** This review will be centered around the work that has been reported on the development of metal–organic frameworks (MOFs) serving as catalysts for the conversion of carbon dioxide into short-chain hydrocarbons and the generation of clean energies starting from biomass. MOFs have mainly been used as support for catalysts or to prepare catalysts derived from MOFs (as sacrifice template), obtaining interesting results in the hydrogenation or oxidation of biomass. They have presented a good performance in the hydrogenation of CO<sub>2</sub> into light hydrocarbon fuels. The common patterns to be considered in the performance of the catalysts are the acidity of MOFs, metal nodes, surface area and the dispersion of the active sites, and these parameters will be discussed in this review.

**Keywords:** metal–organic frameworks; heterogeneous catalysis; carbon dioxide; biomass; hydrogenation; oxidation; Fisher-Tropsch



**Citation:** Valdebenito, G.; González-Carvajal, M.; Santibañez, L.; Cancino, P. Metal–Organic Frameworks (MOFs) and Materials Derived from MOFs as Catalysts for the Development of Green Processes. *Catalysts* **2022**, *12*, 136. <https://doi.org/10.3390/catal12020136>

Academic Editors: José Ignacio Lombrana, Héctor Valdés and Cristian Ferreiro

Received: 31 December 2021

Accepted: 19 January 2022

Published: 22 January 2022

**Publisher's Note:** MDPI stays neutral with regard to jurisdictional claims in published maps and institutional affiliations.



**Copyright:** © 2022 by the authors. Licensee MDPI, Basel, Switzerland. This article is an open access article distributed under the terms and conditions of the Creative Commons Attribution (CC BY) license (<https://creativecommons.org/licenses/by/4.0/>).

## 1. Introduction

In recent years, the world has seen a significant increase in temperature due to different pollutants present in the atmosphere. These pollutants are responsible for the famous greenhouse gas effect [1]. CO<sub>2</sub> is one of the pollutants found in greater concentration in the atmosphere and its emission is mainly due to the use of fossil fuels (heating, automobiles, industrial chimneys) [1,2]. Today there are many proposals to generate a cleaner and healthier environment for living, but one of the proposals that attract the most attention is the conversion of CO<sub>2</sub> to hydrocarbon molecules, which can later be used as fuel in different areas [3–5]. This proposal largely solves the problem of atmospheric pollution on the planet and opens up new areas for the development and research of renewable energies [4].

One of the main problems found in the conversion of CO<sub>2</sub> into hydrocarbon is the need for high-energy processes [5]. Different chemical processes have been investigated that can help to implement a fast and cheap process for the synthesis of renewable energies from CO<sub>2</sub>, such as the use of different types of raw material catalysts [6].

In the last few decades, the valorisation of biomass has garnered great interest. This is due to the fact that by using biomass, one is able to obtain valuable chemical products and sustainable biofuel. The production of this kind of product aims to complement conventional energy sources, especially fossil fuel used in most types of transport [4]. Biomass can be classified into two groups: edible, which is rather scarce, and the much more abundant non-edible biomass. Among the edible kind, we find starch and oils, which are created by processing oilseeds such as rapeseed, miscanthus or soy, and can be transformed into biofuel, also known as biodiesel [7]. This fuel can also be produced from recycled oils obtained from food and gastronomic industries. Fat acids in the oils from both sources, fresh and recycled, are converted into biodiesel by going through a transesterification process that, along with the esters corresponding to the biodiesel, yields

glycerol, a compound that is produced in quantities exceeding its industrial demand [8]. Because of this, the refining and upgrading of glycerol are desirable in order to prevent this by-product from turning into waste and harnessing the biomass completely [8]. Glycerol is considered a platform compound, that is, a chemical species from which other species with added value can be formed, such as diols or glycerol carbonate, which are used in various industries. However, the chemical reactions involved in the conversion of glycerol usually need to be carried out in the presence of a catalyst. It is common to use homogeneous catalysts for these reactions [9].

With respect to the non-edible biomass, the most abundant is lignocellulose. It is part of the structural basis of every plant, so it can be obtained from crops, farming waste or forest waste [10]. Lignocellulosic biomass is divided into three parts: cellulose, hemicellulose and lignin, and for their separation, different methods have been employed, such as thermal methods, pyrolysis or gasification, all of which require high amounts of energy and are not very selective [10]. Fermentation is a more selective method, but it is not efficient in terms of yield. The catalytic conversion of biomass is a better method since the chemical specificity of catalysts enhances the selectivity and, when used in optimal conditions, can also enhance the yielding rate while reducing the required energy [11].

Heterogeneous catalysts are the most used for the conversion of lignocellulosic biomass, particularly supported catalysts. This kind of material consists of a catalytically active molecule, mostly transition metal species, hosted into the structure of a different and chemically stable material known as the support [12,13]. Different compounds have been used as support, such as alumina, zeolites or activated carbon. This provides supported catalysts with an augmented surface area, which improves the substrate/catalyst interaction [14,15].

Another kind of catalyst is that of coordination polymers, among which metal–organic frameworks (MOFs) are the most used. MOFs are classified within the group of porous materials. These compounds are formed by two important parts that define the structural base: the inorganic moiety and the organic linker [16]. The inorganic part corresponds to the metallic center, which presents simultaneous coordinated bonds with different ligands of organic nature. The structure of these species presents porosity, which is the fundamental characteristic of metal–organic frameworks. The existence of pores is mainly due to the geometrical network that is formed between the bonds of the organic ligands and the metallic centres. The length of the organic ligands and the extensive bonds formed with the metallic centres contribute greatly to the size and diameter of the pores present in the MOF, thus determining the catalytic activity [16,17]. On the other hand, the volume of the pores and the specific surface area that these ligands provide in the network characterize MOFs as excellent immobilizers for molecular catalysts.

The physical and chemical characteristics of these compounds can be modified, as different types of MOF can be formed by using different metallic centres and organic ligands, thus generating greater selectivity towards a certain chemical reaction. All these properties allow the synthesis of a wide range of compounds with different characteristics, which will help to choose the most suitable type of MOF for various reactions [3–5]. Regarding the organic ligands used for the synthesis of MOFs, the most common are polyamines, phosphonates, crown ethers and carboxylates (Figure 1) [16].

The use of these compounds is quite varied because they can become very versatile or specific, depending on the area in which their use is required. Some of the applications can be as adsorbent materials in aqueous solutions, due to their properties and structural characteristics, in addition to the low cost [18]. Within the novel research and technologies related to the use of new types of energy from renewable sources, the use of MOFs as electrochemical capacitors and in fuel electrodes for rechargeable batteries has been developed [17].

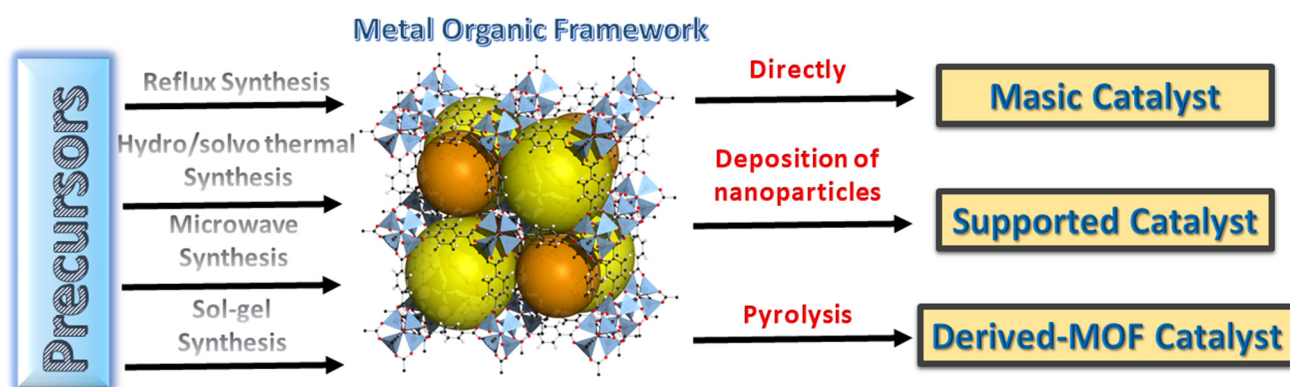


**Figure 1.** Summary of main routes to obtain catalysts based on MOFs.

Besides, the structure and pores of MOFs can be modified by post-synthetic procedures that allow the material to be more selective, determining greater efficiency in the CO<sub>2</sub> adsorption process; these modifications lead to an efficient catalytic process [18–21]. The use of MOFs in heterogeneous catalysis has been of great importance due to their physical and chemical properties; these greatly improve the parameters necessary to be considered for a useful catalyst [18]. The properties of MOFs that stand out are the high thermal stability, the high porosity that serves as an active site for chemical reactions and the enormous regenerative capacity that allows the reuse of these compounds, which finally lead to a lower total cost for the catalytic reactions [19]. Altering the structure of a MOF is not such a complex process and it facilitates the addition of different ligands to the structure, thus making the network more useful in different scenarios, such as the solution medium in which the reaction is taking place [20,21]. These processes allow MOFs to be used in many areas, such as electrocatalysis, photocatalysis and biocatalysis [22–24].

Different ways of covering the need to create and use various types of renewable energies, such as fuels and biofuels, by the use of CO<sub>2</sub> and biomass as the main raw material will be highlighted in the following sections. For the synthesis and chemical conversion of CO<sub>2</sub>, catalysts will be mentioned based on the properties of metal–organic frameworks, which affect different variables that significantly reduce the reaction parameters. In this way, MOFs are shown to decrease the monetary and energy costs of the processes, which are involved in the transformation of CO<sub>2</sub> and biomass into valuable products.

## 2. MOFs for Conversion of CO<sub>2</sub> into Light Hydrocarbons Fuels

Carbon dioxide is a very stable molecule, comparable to water ( $\Delta G^\circ_f = -396$  kJ/mol). Due to this fact, the use of CO<sub>2</sub> as a precursor to obtaining valuable products requires high energy; especially CO<sub>2</sub> conversion to light hydrocarbon fuels (LHCF) [25,26].

An excellent alternative to producing renewable fuels starting with CO<sub>2</sub> is using catalysts, thus reducing the carbon footprint of the processes. The heterogeneous catalysts offer an alternative to decreasing the high activation energies associated with CO<sub>2</sub> activation to produce renewable fuels. Zeolites, oxides, nanoparticles and supported catalysts have shown promising results in the preparation of LHCF by CO<sub>2</sub> reduction. This type of catalyst is capable of controlling the selectivity to methane, C<sub>2</sub>–C<sub>8</sub> paraffins and olefins, with a detriment in the production of CO [27–35].

MOFs have been shown to be very active catalysts; they are useful in different chemical reactions to produce valuable products. [36–39]. However, in this particular field, they have not been used very often, despite having many attractive characteristics for the conversion, for example, of CO<sub>2</sub> into LHCF. These characteristics include a high surface area, high pore size, Brönsted acid sites and a well-defined position of the active sites in the crystalline network.

Several researchers have worked using MOFs in CO<sub>2</sub> conversion into LHCF [40–43]. Generally, in these reactions, MOFs have been used as supporting material or to manufac-

ture MOF-derived catalysts by pyrolysis. Particularly, the generation of MOF-derived catalysts by pyrolysis offers interesting characteristics when compared to the classical supported catalysts, that is, high dispersion of the active sites, thermal stability and surface area.

The performance, benefits and future perspective of the use of MOFs or MOF-derived catalysts to produce light hydrocarbon fuels starting with CO<sub>2</sub> will be presented and commented on in the following section.

### 2.1. MOFs Used as Supporting Materials for Catalysts

As stated above, MOFs have been used as supports for catalysts, which are then utilized to convert CO<sub>2</sub> into LHCF. One of the most studied catalytic systems is metallic nanoparticles (NPs) supported on MOFs since the porous nature of MOFs permits them to accommodate the NPs.

Hu et al. [44] prepared five catalysts based on MIL-53(Al) and ZIF-8(Zn), using different modifications in the syntheses in order to obtain a variety of morphologies. All catalysts were charged with  $\alpha$ -Fe<sub>2</sub>O<sub>3</sub> NPs. The most remarkable point was that, despite the conversion for all catalysts being lower than 30%, the selectivity to hydrocarbons was very high, between 75–80%. Additionally, the performance of the MOFs as the supporting material was compared against  $\gamma$ -Al<sub>2</sub>O<sub>3</sub> and  $\alpha$ -Fe<sub>2</sub>O<sub>3</sub> (without support) as control reactions. The results showed clear differences associated with user support; the conversion and the selectivity to hydrocarbons were higher when using MOFs as support than that of the controls. Moreover, when comparing the two MOFs, it was possible to observe some differences relative to the produced amount of methane and olefins. It became evident that the selectivity was sensible to the acidity of the MOF used in each catalytic reaction. Moreover, the conversion was also modulated by the morphology of the corresponding MOF and particle size of the catalyst and surface area. The surface area was 1535 m<sup>2</sup> g<sup>-1</sup> for MIL-53(Al) and 1918 m<sup>2</sup> g<sup>-1</sup> for ZIF-8(Zn), with ZIF-8(Zn) being more active than MIL-53(Al) as a catalyst.

Tarasov et al. [45] used MIL-53(Al) as support, but they embedded the material with Co NPs as active metal sites. The obtained results were similar to those obtained by Hu et al. [44]; the conversion was between 25–38% and the selectivity to hydrocarbons was 74–91%. The study focused on the effect of the reaction conditions, mainly the temperature, which ranged from 260 to 340 °C. As the temperature was raised, the conversion and the selectivity increased. The amount of methane increased with higher temperatures, while the obtained amount of C<sub>2</sub>–C<sub>5</sub> and C<sub>5+</sub> was reduced. The Brønsted acid sites present in the catalyst permitted the regulation of the relationship between paraffins and olefins. The proposed mechanism related to this catalytic reaction assumed that the Co NPs generated interactions with CO<sub>2</sub>, thus reducing it to CO. This step was followed by the Fisher-Tropsch reaction (FTR), which produced light hydrocarbons (Figure 2).

The hydrogenation of CO<sub>2</sub> was studied by Zhao et al. [46] using a Zr-based metal-organic framework, Zr<sub>6</sub>O<sub>4</sub>(OH)<sub>4</sub>(BDC)<sub>6</sub> (UiO-66) (BDC = 1,4-benzenedicarboxylate), as support for Ni NPs generated by an in situ reduction, obtaining highly monodispersed ultra-small nanoparticles (1.6–2.6 nm) (Ni@UiO-66). The catalysts were prepared by modifying the load of Ni NPs from 5 to 30 wt%. The dependence of the conversion with temperature was studied for the hydrogenation of CO<sub>2</sub> to CH<sub>4</sub>; the highest conversions were achieved when the loadings were 20, 25 and 30 wt% at 340 °C. The selectivity was tested for a reaction time of 100 h at 300 °C, using a load of 20% (20Ni@UiO-66), obtaining 58% of conversion and 100% of selectivity to CH<sub>4</sub> [46].

A similar study by Zhen et al. [47] reported the synthesis of Ni@MIL-101 with the same loadings of Ni NPs. The catalyst had a high surface area of 3297 m<sup>2</sup> g<sup>-1</sup>, which showed an excellent performance to methanation of CO<sub>2</sub>, achieving 100% of the conversion with a 100% selectivity to CH<sub>4</sub> at 300 °C. On the other hand, Zhen et al. [48] also used MOF-5 as support for Ni NPs. The catalyst exhibited a surface area of 2961 m<sup>2</sup> g<sup>-1</sup> at 300 °C; the conversion was 57%, obtaining exclusively CH<sub>4</sub> (Table 1).

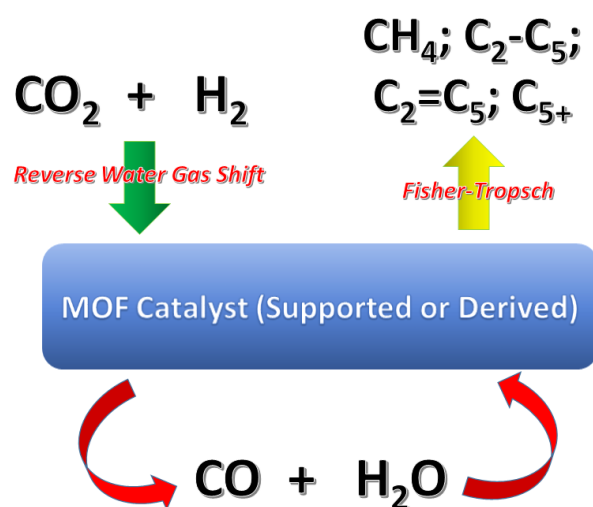


**Figure 2.** Scheme of the reactions to convert  $\text{CO}_2$  in LHCF using MOFs as catalysts.

**Table 1.** Summary of catalytic results for the hydrogenation of  $\text{CO}_2$  with different supported catalysts.

Catalyst	$\text{CO}_2$ Conversion (%)	Mass of Catalysts (g)	Temperature ( $^\circ\text{C}$ )	Selectivity (%)					Reference
				CO	$\text{CH}_4$	$\text{C}_2\text{-C}_4^-$	$\text{C}_2\text{-C}_4^=$	$\text{C}_5^+$	
MIL-53(Al)/ $\text{Fe}_2\text{O}_3$	20	1	300	20	41	34	0	5	[44]
ZIF-8(a)(Zn)/ $\text{Fe}_2\text{O}_3$	23	1	300	23	21	23	21	12	[44]
ZIF-8(b)(Zn)/ $\text{Fe}_2\text{O}_3$	25	1	300	21	22	30	15	12	[44]
ZIF-8(c)(Zn)/ $\text{Fe}_2\text{O}_3$	30	1	300	17	25	40	8	10	[44]
10%Co/MIL-53(Al)	25	0.8	260	26	26	22	0	26	[45]
10%Co/MIL-53(Al)	30	0.8	300	19	28	24	0	28	[45]
10%Co/MIL-53(Al)	38	0.8	340	9	32	27	0	32	[45]
5Ni@UiO-66	8	0.1	300	#	#	#	#	#	[46]
10Ni@UiO-66	13	0.1	300	#	#	#	#	#	[46]
15Ni@UiO-66	25	0.1	300	#	#	#	#	#	[46]
20Ni@UiO-66	58	0.1	300	100	0	0	0	0	[46]
25Ni@UiO-66	50	0.1	300	#	#	#	#	#	[46]
30Ni@UiO-66	41	0.1	300	#	#	#	#	#	[46]
20Ni@MIL-101	100	0.2	300	100	0	0	0	0	[47]
10Ni@MOF-5	57	0.2	300	100	0	0	0	0	[48]

# The authors do not give information about the selectivity.

The hydrogenation of  $\text{CO}_2$  can also produce MeOH. The generation of MeOH, starting from  $\text{CO}_2$ , was tested by Somorjai et al. [49] using Cu NPs (18 nm) over two different MOFs as support, UiO-66, MIL-101 and ZIF-8. The reactions were carried out at 175  $^\circ\text{C}$  and 0.4 g of the catalyst. The results were interesting since only CuUiO-66 was able to catalyze the reaction, obtaining 5% conversion and 100% selectivity. The X-ray photoelectron spectroscopy data obtained on the surface of the catalyst showed the presence of Zr oxide clusters or Zn oxides generated a strong interaction with the Cu NPs. This interaction allowed the coexistence of different oxidation states of copper, which play different roles in the mechanism of the production of methanol.

In a similar way, Lin et al. [50] developed Cu/ZnOx NPs supported on UiO-bpy in order to take advantage of the synergistic interaction that occurs between copper and zinc. The reaction was conducted at 250  $^\circ\text{C}$  and 0.1–0.3 g of catalyst; the conversion was 17.4% and the selectivity to MeOH was 85.6%. The importance of the Zn was demonstrated using only Cu in the reaction; the performance of the catalyst decreased. On the other hand, a TPD of  $\text{CO}_2$  study revealed that the vacancies or unsaturated Zr sites of the support (UiO-bpy) interact with the  $\text{CO}_2$  in the catalytic cycle. These open sites can adsorb  $\text{CO}_2$  and accept dissociated hydrogen atoms to form Zr-H, likely playing a key role in catalytic  $\text{CO}_2$  hydrogenation.

## 2.2. Catalysts Obtained by Pyrolysis of MOFs

Another synthetic route to obtaining heterogeneous catalysts for CO<sub>2</sub> activation is the preparation of these by pyrolysis of MOFs. Several papers can be found in the literature reporting this technique, and these will be summarized in this section.

Liu et al. [51] synthesized Fe-based catalysts by pyrolysis of Fe-MIL-88. The catalysts contained a high load of Fe, in comparison with classical supported catalysts. The authors controlled the temperature and the time of the syntheses of these catalysts, with the loading of Fe in the obtained catalysts resulting between 34–51%. The used conditions in the preparation of these catalysts affected the mean particle size and dispersion. The authors remarked that the dispersion of the active sites was more homogeneous than in the classical supported catalysts. The results were promising; the best performance was achieved with a 46% conversion and 82% selectivity to light hydrocarbons, with C<sub>2</sub>–C<sub>4</sub> paraffins (34%) being the main products. Compared with the aluminum oxide supported catalysts, these MOF-derived catalysts were capable of obtaining higher CO<sub>2</sub> conversion and better selectivity of valuable products. The MOF-derived catalysts showed larger stability than aluminum oxide supported catalysts due to the high dispersion of metal particles in the matrix.

Another Fe-based catalyst was synthesized by pyrolysis of (Fe-BDC) MOF (BDC = 1,4-benzenedicarboxylate). The hydrogenation of CO<sub>2</sub> after 12 h of reaction was promoted by sodium, together with the MOF-derived catalyst (Na-Fe@C). The catalyst exhibited interesting results, showing a conversion close to 40% and a selectivity of 80% to hydrocarbons, with C<sub>5+</sub> as the main product [52]. The authors also proposed a combination of hierarchical zeolite H-ZSM-5 with the prepared MOF-derived catalyst, expecting to obtain aromatics as the main products. The acid environment contributed by the zeolite did not produce significant changes in the conversion; however, the new reaction environment permitted the isolation of aromatic compounds. Moreover, the aromatic compounds were the main products of the catalytic reaction. Different concentrations of zeolite were tested and compared, and the most active one used 0.2 M of H-ZSM-5 together with Na-Fe@C, with selectivities close to 30% for C<sub>5+</sub> and 42% for aromatic compounds.

A similar process was tested by Martin, Dusselier et al. [53] by combining a chabazite-type zeolite (CHA) with In-ZrMOF, starting from (Zr)UiO-67-bipy-In, which was calcined at 580 °C for 5 h. The new material presented good dispersion and strong acidity, which allowed for the couple activation of CO<sub>2</sub>. The catalytic reaction was carried out at 375 °C, and the products were obtained with space–time yields of 0.1 mol of CO<sub>2</sub> converted to light olefins per gram of In per hour. However, the selectivity to CO was high at 70%, and the remaining 30% was distributed between olefins (25%), with several minor products also distributed among paraffins (2%), methane (2%) and oxygenated products (1%). In this case, the acidity of the material allowed the breaking of the C–O bond, thus activating CO<sub>2</sub>. Nevertheless, the following step corresponding to the hydrogenation of CO<sub>2</sub> was not successful due to the high amount of reported CO.

Ramirez et al. [54] reported the preparation of several catalysts by pyrolysis of Basolite F300 (Fe-MOF). These catalysts contained a loading of ca. 41% of Fe. The set of catalysts was prepared by the addition of 0.75% of fourteen different promoters and was used to evaluate the improvement of the reverse water gas shift (RWGS) activity (Fe, Cu, Mo, Rh, Pt, Ni) [55–60] or olefin selectivity (Li, Na, K, Mg, Mn, Ca, Zn, Co) [61–65]. The results permitted us to conclude (Table 2) that the use of the different metals as promoters could activate or inhibit the reaction. For example, K, Pt and Cu activated the reaction, increasing the conversion in comparison with the used control catalysts. In contrast to the catalysts without promoters, with Mo, Ca and Mn, the conversion decreased.

**Table 2.** Summary of catalytic results of Fe/C catalysts using different metals as promoters at 320 °C.

Catalyst	Conv. (%)	Selectivity (%)				
		CO	C <sub>1</sub>	C <sub>2</sub> –C <sub>6</sub>	C <sub>2</sub> =C <sub>6</sub>	C <sub>7+</sub>
Fe/C	24	39	39	12	1	9
Fe/C + Fe	25	40	38	12	1	9
Fe/C + Cu	29	23	53	15	2	7
Fe/C + Mo	22	50	30	9	1	10
Fe/C + Li	26	38	40	12	2	8
Fe/C + Na	27	38	32	15	4	11
Fe/C + K	35	17	18	7	40	18
Fe/C + Mg	22	48	39	9	1	3
Fe/C + Ca	24	40	43	13	1	3
Fe/C + Zn	23	41	45	13	1	0
Fe/C + Ni	26	34	52	13	1	0
Fe/C + Co	26	32	51	14	2	1
Fe/C + Mn	23	45	38	8	1	8
Fe/C + Pt	30	22	51	19	3	5
Fe/C + Rh	25	17	63	19	1	0

The best promoters were K for the olefin selectivity and Rh for the RWGS reaction, while the worst was Mo for this same reaction. The metals that resulted as promoters considerably enhanced the selectivity towards hydrocarbons, varying it between 83% and 50%. Thus, the most active catalyst was that which contained K as promoter (conversion 35% and selectivity 83%). Furthermore, when this catalyst was used, a higher amount of olefins (C<sub>2</sub>–C<sub>6</sub>) was obtained. The reaction conditions using this catalyst were investigated, modulating the loading of K, the temperature of the reaction and time. The reaction time did not present a significant effect and the loading of K did not change the conversion when the loading was above 0.75%, while a lower loading of K decreased the conversion and selectivity to HC. Finally, the optimal temperature resulted at 375 °C, achieving 40% of conversion. Data corresponding to the catalytic reactions carried out at 320 °C are summarized in Table 2.

Pyrolyzed MOFs have also been used in methanation reactions. From pyrolyzed ZIF-67 (Co), Co-xH<sub>2</sub>/Ar was obtained with a surface area of 125 m<sup>2</sup> g<sub>Co</sub><sup>-1</sup>. [66]. The methanation reaction was conducted at 300 °C; the conversion achieved a 48.5% with a 97% of selectivity to CH<sub>4</sub>. In the same way, Ni@C was prepared by pyrolysis of Ni-MOF, and the surface area was shown to be 177 m<sup>2</sup> g<sup>-1</sup>. The temperature dependence of the reaction was studied, and the conversion achieved 100% when the temperature of the reaction exceeded 300 °C, with 100% selectivity [67]. Additionally, to understand the reaction mechanism, in situ DRIFTS spectra were recorded, in order to show the catalyst co-interacting with CO<sub>2</sub> and H<sub>2</sub> at different temperatures (between 50 to 400 °C). From the results, it was possible to conclude that an intermediary species, Ni–CO<sub>2</sub>, was formed due to the interaction between the catalyst and CO<sub>2</sub>, followed by the reaction of dissociated H to form Ni–C–(OH)<sub>2</sub> intermediates. These intermediates continued reacting with dissociated H to produce CH<sub>4</sub> and H<sub>2</sub>O.

### 2.3. Perspectives and Conclusions

The generation of renewable fuels from CO<sub>2</sub> is a field intensely explored in recent years. However, the direct use of MOFs as catalysts for this reaction is scarce and opens up a great perspective of possibilities, mainly in the generation of light hydrocarbon fuels from CO<sub>2</sub>. The recent reports discussed in this work show the first steps that have been taken in this area, with interesting and promising results. Two strategies have been used to convert CO<sub>2</sub> in LHCF: MOFs used as supporting material for catalysts, and catalysts obtained by pyrolysis of MOFs.

When MOFs are used as support, the intrinsic characteristics of MOFs are more determinant in the result, modulating the conversion and the selectivity by surface area,

dispersion or/and acidity. Moreover, the acidity of the support modulates the selectivity, for example, the ratio between the obtained olefins and the paraffins. It is important to consider that, at the time of designing a MOF as support, the use of a metal ion that will provide an acidic environment has to be considered in order to increase the production of hydrocarbons over CO. Additionally, the utilization of specific organic linkers, which will increase the porosity and the surface area and directly affect the conversion in these processes, has to be also evaluated.

On the other hand, the use of MOFs to prepare catalysts by pyrolysis will completely change the original properties of the MOF. Moreover, the obtained new catalyst will present high dispersion, low particle size and high surface area. The main point in the design of the MOF is the selection of the active metal ion. The cited authors have used Fe or Co to prepare this type of catalyst due to the fact that these metals are active in the RWGS and the Fisher-Tropsch reaction.

An unexplored way to face these reactions is to directly test MOFs as catalysts, combining the acidity of an active metal ion and the organic linkers that will generate high surface areas. The combination of metals ions to produce bimetallic MOFs may also be a promising area of focus to enhance the conversion and the selectivity to LHCF. Moreover, these bimetallic MOFs may also be used in pyrolysis processes in order to obtain new bimetallic nanoparticles with high dispersion, activity and selectivity.

In summary, MOFs have shown promising results, presenting high selectivity to LHCF. Nevertheless, they have not been extensively used in this field and, therefore, remain an open field of research. The use of catalysts is very important to generate sustainable processes to convert CO<sub>2</sub> into hydrocarbons, decreasing the carbon footprint and helping to mitigate the greenhouse effect. The use of MOFs in these catalytic reactions still presents many challenges, thus opening a number of new areas of research.

### 3. MOFs and Their Application in Hydrogenation and Oxidation Reactions for Biomass Valorisation

This section will discuss the structural and chemical properties of MOFs, which must be considered when choosing them as support or catalysts for biomass upgrading reactions.

#### 3.1. Hydrogenation

Platform compounds found in biomass can undergo diverse transformations depending on the type of reaction in which they are involved. Hydrogenation or reduction reactions are useful to obtain alcohol from carbonyl compounds [68] or saturated hydrocarbons by cleavage of C–O bonds [69,70]. Herein, we present the properties of MOFs, which directly influence the behaviour of hydrogenation reactions of biomass platform compounds (Figure 3).

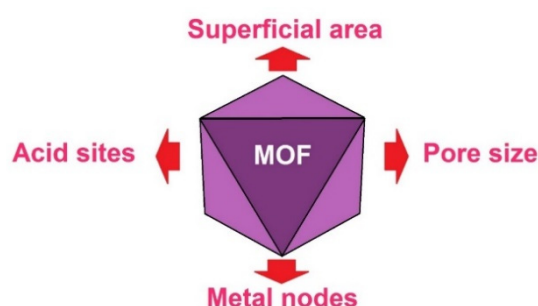


**Figure 3.** Relevant parameters to be considered in the preparation of MOFs, which will be used as catalysts in biomass transformation.

##### 3.1.1. Surface Area and Pore Size

Ruiqi et al. [68] reported the use of MOFs designated as UiO-66 and H-UiO-66 as support for different transition metal nanoparticles (Au, Pt, Cu and Pd). These materials

were used as heterogeneous catalysts in the hydrogenation of furfural, using molecular hydrogen to obtain furfuryl alcohol. The best results were achieved in relatively mild conditions (60 °C and 0.5 Mpa) using water as solvent and Pd/H-UiO-66 as the catalyst, yielding a complete conversion and >99% selectivity to furfuryl alcohol with a TOF of 66.7 h<sup>-1</sup>. These good results are attributable to the high dispersion and uniform distribution of the nanoparticles (NPs) over the highly porous MOF. This allows reducing the mass diffusion resistance and grants great accessibility for the substrate to interact with the active sites of the catalyst (Pd NPs). ATR-IR spectroscopy showed that the principal interaction between the substrate and the catalyst occurred through the C=O and C=C bonds (stretching bands at 1670 cm<sup>-1</sup> and 1540 cm<sup>-1</sup>, respectively), which explains the high selectivity of the catalytic system [71]. Since the hydrogenation of the carbonyl group of furfurals is necessary for alcohol formation, the interaction between carbonyl groups from the substrate and the Pd NPs from the catalyst is fundamental for high conversion and selectivity [72].

Yuan et al. [71] also studied MOF UiO-66 as a support for several metallic NPs. The obtained results indicated that the best catalyst was Ru/UiO-66, which showed a furfural conversion of 94.9% with 100% selectivity to furfuryl alcohol. The Ru/UiO-66 catalyst presented the highest surface area, as compared to the other catalysts studied in this work. Another interesting feature was that the Ru NPs in the catalyst were oxidized in contact with air. However, the obtained RuOx species were again reduced under the reaction conditions, giving rise to the active sites for the hydrogenation of the substrate. The authors suggest that the good results obtained were attributed to the small size of the Ru NPs (less than 3 nm), the interaction of the Ru NPs with the support and the redox properties of the RuOx species.

Jian et al. [73] used Pd@UiO-66, Pd@UiO-66-NH<sub>2</sub> and Pd/UiO-66-NH<sub>2</sub> in the catalytic hydrogenation of levulinic acid (LA) to obtain  $\gamma$ -valerolactone (GVL). Results showed that a good dispersion of Pd NPs throughout the MOF improves the conversion. The worst dispersion was found in Pd/UiO-66-NH<sub>2</sub> where Pd NPs were located along the edges of the MOF instead of inside the MOF. This, because the traditional impregnation technique yields Pd NPs with a 5.8 nm diameter, was too big to penetrate the MOF structure. On the other hand, Pd@UiO-66 and Pd@UiO-66-NH<sub>2</sub> were synthesized with a double solvent method, using water and n-hexane [74], which produced Pd NPs with a mean particle size of 1.1 nm, thus enabling them to enter the MOF structure. This procedure enhanced the dispersion of the NPs. It is worth noting that the NH<sub>2</sub> group had a notorious influence on the loading of Pd contained within the MOF [75]. The percentage of Pd present in the catalyst was determined by ICP-AES, showing a 0.57% for Pd@UiO-66, and 0.94% Pd@UiO-66-NH<sub>2</sub> (with an expected theoretical value of 1%). These results were explained by the coordinating capacity of the -NH<sub>2</sub> group, which retained the Pd NPs inside the MOF. Under the selected conditions for the catalytic studies, Pd@UiO-66-NH<sub>2</sub> presented the best results both in structural properties, including Pd loading and dispersion, and in catalytic activity, converting 98.2% of the substrate with a selectivity of 100% towards the GVL after 2 h of reaction (hydrogen pressure, 2 MPa; temperature, 140 °C).

The proposed mechanism for the transformation of lactic acid to GVL sets the necessity of sites that allow the activation of hydrogen and acid sites, including both Lewis and Brønsted, which promote the LA dehydration. The Pd NPs take care of the first step, activating the hydrogen when it disperses and adsorbs on them, while the Zr<sub>6</sub> clusters generate the Lewis and Brønsted acid sites that interact with the -OH group from the LA [76–78]. When both molecular hydrogen and LA have interacted with the catalyst, the first hydrogenation step occurs, producing 4-hydroxipentanoic acid adsorbed in the NP@MOF system, followed by acid catalysed dehydration allowing the intramolecular esterification thus yielding GVL [73]. This proposed mechanism remarks the importance of good NPs dispersion along the MOF structure since it is a determinant for the hydrogenation step. Another relevant factor is the existence of the acid sites present in the MOF

structure, which makes possible not only the activation of LA but also the final dehydration step, which is a common important factor in biomass upgrading reactions.

### 3.1.2. Acidity

As mentioned, acid sites play a very important role in the properties of a catalyst. For example, Xiang et al. [79] studied the chemical transformation of furfuryl alcohol into 4-hydroxi-2-cyclopenthenol (HCP) and 2-cyclopenthenone (CPE), using FeZn, FeZn-P, Cr-MIL-101 and Fe-MIL-100 as catalysts. The Lewis acid sites are necessary for this reaction since the substrate–catalyst interaction occurs on these sites to promote dehydration, aldol condensation and hydrogenation of the substrate. In the FeZn and FeZn-P catalysts (double-metal cyanide kind of MOFs or DMC), the Zn<sup>II</sup> ions correspond to the acid sites, while for Cr-MIL-101 and Fe-MIL-100, the Cr<sup>III</sup> and Fe<sup>III</sup> are the acid sites, respectively. The catalysts acidity was determined by FT-IR, measuring the absorption bands of pyridine chemisorbed on the Lewis (1450 cm<sup>-1</sup>) and Brönsted (1540 cm<sup>-1</sup>) acid sites [80]. This study determined that both FeZn and FeZn-P catalysts presented a Lewis/Brönsted acid site density ratio of 10.2 and 12.8, respectively, while Cr-MIL-101 and Fe-MIL-100 only presented the Lewis acidity with acid site densities of 2790 and 3072 mmol·g<sup>-1</sup>, respectively [79].

For the transformation of furfuryl alcohol, Brönsted acids such as H<sub>2</sub>SO<sub>4</sub>, HCl, *p*-toluensulfonic acid, H-ZSM-5 (an acidified commercial zeolite), hyaluronic acid or Amberlyst-15 (a strongly acid exchange resin) readily catalyse the hydrolysis reaction, favoring the production of levulinic acid [81,82]. For example, when using Amberlyst-15, only a 16.5% selectivity towards the HCP is achieved, yielding mostly levulinic acid as the product. On the other hand, all the catalysts used by this research group presented Lewis acid sites and exhibited higher yields for the HCP product. Cr-MIL-101 and Fe-MIL-100 presented a relatively lower conversion, being below 85%, with selectivity values ca. 70% versus 88.8% of conversion (approximately 86% selectivity towards HCP) achieved with FeZn, and 95.2% conversion (96.2% selectivity towards HCP) achieved with FeZn-P. This behaviour was attributed to the weaker acidity of Cr<sup>III</sup> and Fe<sup>III</sup> ions as compared to that of the Zn<sup>II</sup> ions.

When comparing the two DMC catalysts, the better results obtained for FeZn-P are attributed, according to the authors, to the higher surface area (42.6 m<sup>2</sup>·g<sup>-1</sup>) and acid density (1349 mmol·g<sup>-1</sup>). However, it is worth noting that while Fe- and Cr-based catalysts present surface areas 20 and 70 times higher than that of FeZn-P and higher Lewis acid densities as well, their conversions and selectivity still remain lower than FeZn-P. This may be related to the absence of Brönsted acidity in Cr-MIL-101 and Fe-MIL-100, which would have a significant impact on the catalytic activity of both materials in the furfuryl-alcohol conversion.

The two DMC catalysts were used to study the conversion of furfuryl alcohol to CPE, using from 2 to 6 MPa, augmenting the CPE yield from 20.4% to 61.5%, the highest achieved conversion. This indicates that the DMC materials can be used as acid catalysts and hydrogenation catalysts. The authors point out that DMC catalysts have been primarily used as acid catalysts, so, by being active in hydrogenation catalysis, they become bifunctional catalysts for both types of reactions. This was corroborated with the study of the furfuryl alcohol conversion to CPE using other catalysts in the presence of molecular hydrogen. The acid catalysts Amberlyst-15 and Al-MCM-41 were not able to catalyse this reaction, while the bifunctional DMC and MIL catalysts reported in this work displayed a considerable CPE yield with the used experimental conditions, thus confirming the necessity of both acid and hydrogenation catalytic active sites.

A point worth considering is the fact that the acidity of a MOF can be modified with post-synthetic methods, such as the dispersion of Brönsted acid molecules (for example, sulfuric or phosphoric acid) throughout the MOF. Phosphoric acid, for example, is able to host inside the pores of MIL-101, enhancing its activity in the catalytic hydrodeoxygenation of biomass oleic acid to yield saturated hydrocarbons [68]. In this work, the concentrations of phosphoric acid dispersed in the Pt@MIL-101 supported system were varied, resulting

in a dramatic enhancement of the oleic acid conversion from 15% to 57% when the concentration of phosphoric acid was raised from 30 mM to 60 mM. Further increase of the concentration of phosphoric acid produced more discrete augmentations (conversions of 68% and 86.5% for 120 mM and 240 mM, respectively). A higher content of phosphoric acid hosted inside the MIL-101 pores increased the Pt particle size distribution values supported on the MOF. Moreover, the presence of this Brønsted acid had a direct influence on the reaction mechanism, switching from a decarbonylation/hydrogenation system to a hydrodeoxygenation and favouring the production of heptadecane over octadecane.

Another example is presented by Zhang et al. [83], who reported the use of MIL-101-SO<sub>3</sub>H(x) as catalysts (x = 25, 50, 80 and 100) that have different amounts of -SO<sub>3</sub>H groups. These catalysts were studied in the GVL hydrogenation reaction to obtain ethyl valerate, with 98% conversion and 83% selectivity using H<sub>2</sub> at 250 °C for 10 h. The authors mention that the incorporation of a sulfonic acid functional group (-SO<sub>3</sub>H) in the MOF is favorable due to the properties that this group confers to the catalyst, such as strong acidity, favorable textural properties and high hydrothermal stability. The results indicated that a greater number of -SO<sub>3</sub>H acid groups produced a greater conversion of GVL. On the other hand, the obtained good results were attributed to the fact that the palladium supported on the acid materials showed bifunctional catalytic properties, allowing an increase in the density of acid sites. This resulted in increased activity in the opening of the GVL ring and the subsequent hydrodeoxygenation of the C=O bond, allowing the intermediate ethyl pentenoate to be obtained, which was then hydrogenated by the Pd particles to form ethyl valerate.

### 3.1.3. Metal Nodes

The work by Anil et al. [84] indicates that metal node coordination plays an important role in the catalytic activity of a MOF. The catalytic hydrogenation of furfural (FUR) was studied, using Zr-based MOFs (Zr-MOFs) such as UiO-66, UiO-67 and DUT-52 as catalysts, and 2-propanol (2P) as the hydrogen source. The reaction, in absence of the catalyst, presents a conversion under 2%, and from 2% to 5% when carried out in the presence of these Zr-MOFs. The values of conversion do not vary much, whether the reaction is catalysed or not, nor even when the used catalysts are varied, despite the fact that these have different structural properties [85]. While UiO-67 has the highest surface area and pore size, its catalytic activity was not significantly higher than that of UiO-66 or DUT-52, thus indicating that these parameters were not determinant for the catalytic system. However, the number of metal nodes coordinated with carboxylic groups in the unit cell of different MOFs appears to be relevant. When using catalysts with fewer nodes, the conversion is improved. DUT-52 (12 Zr nodes) presented 2.1% conversion, while DUT-67 (8 Zr nodes) had 16.4% and MOF-808 (6 Zr nodes) showed a dramatic increase with 81.3% of conversion for the furfural hydrogenation. This relation between the lower number of nodes and the higher conversion values is explained by the fact that fewer nodes mean more unused space around the metal ions, allowing for better accessibility of the substrate molecules to the active Zr sites, thus yielding higher conversions.

The number of acid and basic sites is another parameter influenced by the number of metal nodes [86,87], and it is determined by TPD-NH<sub>3</sub> and TPD-CO<sub>2</sub>, with MOF-808 presenting the highest values for available acid (0.85 mmol·g<sup>-1</sup>) and basic (0.15 mmol·g<sup>-1</sup>) sites. This is consistent with the fact that MOF-808 is the most active of all the studied Zr-MOFs.

The activation of MOF-808 with methanol modifies the catalyst metal nodes, altering its structure without affecting the crystalline or porous properties of the MOF. This treatment allows the removal of coordinated formate groups, μ<sub>3</sub>-OH and physisorbed DMF, and generates the coordination of methoxy and terminal -OH groups, in addition to forming the coordinatively unsaturated Zr sites, which facilitate the furfural and 2-propanol adsorption on the metal nodes and enhance the catalytic activity. This has been proven by comparing the results obtained for the same experimental conditions (T: 40 °C, t: 24 h, Cat/FUR/2P:

0.1/0.5/12.5) for the hydrogenation of furfural, using the as-synthesized and the methanol activated forms of MOF-808 as catalysts. The activated form surpassed the as-synthesized conversion by over 60% (27.5% versus 96.5%), corroborating the effect of activating the catalysts prior to its use [84].

The methanol activation technique was previously reported by Yang et al. [88], who studied the activation of UiO-66 and Nu-1000, corroborating the formation of methoxy groups on the metal nodes, which modify the surface chemistry of the MOFs. The same author with a different research group [89] made use of this technique for the catalytic dehydration of tert-butyl alcohol. The activated MOF was characterized by FTIR and compared with the as-synthesized material. Two characteristic  $\nu_{C-H}$  absorption bands at  $2931\text{ cm}^{-1}$  and  $2866\text{ cm}^{-1}$ , corresponding to formate groups coordinated to the Zr nodes (Zr-OOCH), disappeared and were replaced by absorption bands at  $2929\text{ cm}^{-1}$  and  $2827\text{ cm}^{-1}$ , corresponding to the  $\nu_{C-H}$  vibrations from methoxy groups coordinated with the Zr nodes (Zr-OCH<sub>3</sub>) [90]. Thus, the substitution of the formate groups by methoxy groups necessary for the activation was confirmed. When analysing the spectrum of the MOF activated with deuterated methanol, it is possible to observe that the methoxy bands are shifted to lower energies ( $2203\text{ cm}^{-1}$  and  $2060\text{ cm}^{-1}$ ), as expected for the  $\nu_{C-D}$  vibration of the deuterated methoxy coordinated group. Using spectral data, it was possible to prove that the generation of these methoxy coordinated groups is in fact produced by the methanol activation method.

The activated M-MOF-808 also proved to be an efficient catalyst in the hydrogenation reaction of carbonylic biomass derivatives to produce alcohols. Among the studied substrates, 5-hydroxymethylfurfural (5-HMF), ethyl levulinate, 5-methylfurfural, benzaldehyde, 4-chlorobenzaldehyde and acetophenone were hydrogenated to their respective alcohols in mild conditions (T:  $82\text{ }^{\circ}\text{C}$ , S/Cat: 0.106), yielding conversions and selectivities above 90%. The summary of the reactions and its catalytic results are shown in the Figure 4 and Table 3.

**Table 3.** Different catalysts and catalytic conditions in hydrogenation reactions for biomass valorisation.

	Catalyst	Catalyst (mg)	Substrate	Substrate (mmol)	Hydrogen Sours	T ( $^{\circ}\text{C}$ )	t (h)	Conv. (%)	Selectivity (%)	Product	Ref.
a	Pd/H-UiO-66	0.3 mol%	FUR	5.0	0.5 MPa H <sub>2</sub>	60	3	100	>99	FOL	[68]
b	Ru/UiO-66	100	FUR	0.1 mL FUR in 9.9 mL H <sub>2</sub> O	0.5 MPa H <sub>2</sub>	20	4	94.9	100	FOL	[71]
c	Pd@UiO-66-NH <sub>2</sub>	150	LA	5	2 MPa H <sub>2</sub>	140	2	98	100	GVL	[73]
d	FeZn-P	100	FOL	10.2	-	150	6	95	88.2	HCP	[79]
	FeZn-P	100	FOL	10.2	4 MPa H <sub>2</sub>	150	6	95	61.5	CPE	
e	Pd/MIL-101-SO <sub>3</sub> H	100	GVL	10	3 MPa H <sub>2</sub>	250	10	98	83	Ethyl valerate	
f <sup>a</sup>	Pt/P@MIL	50	Oleic acid	0.0047 (mmol/s·g <sub>cat</sub> )	2 MPa H <sub>2</sub>	300	2	75	-	HDO products	[70]
g	M-MOF-808	100	FUR	10	IPA <sup>b</sup> 416 mmol	40	24	96.5	88.6	FOL	[84]

<sup>a</sup> Catalysis in gas phase. <sup>b</sup> IPA: 2-propanol.

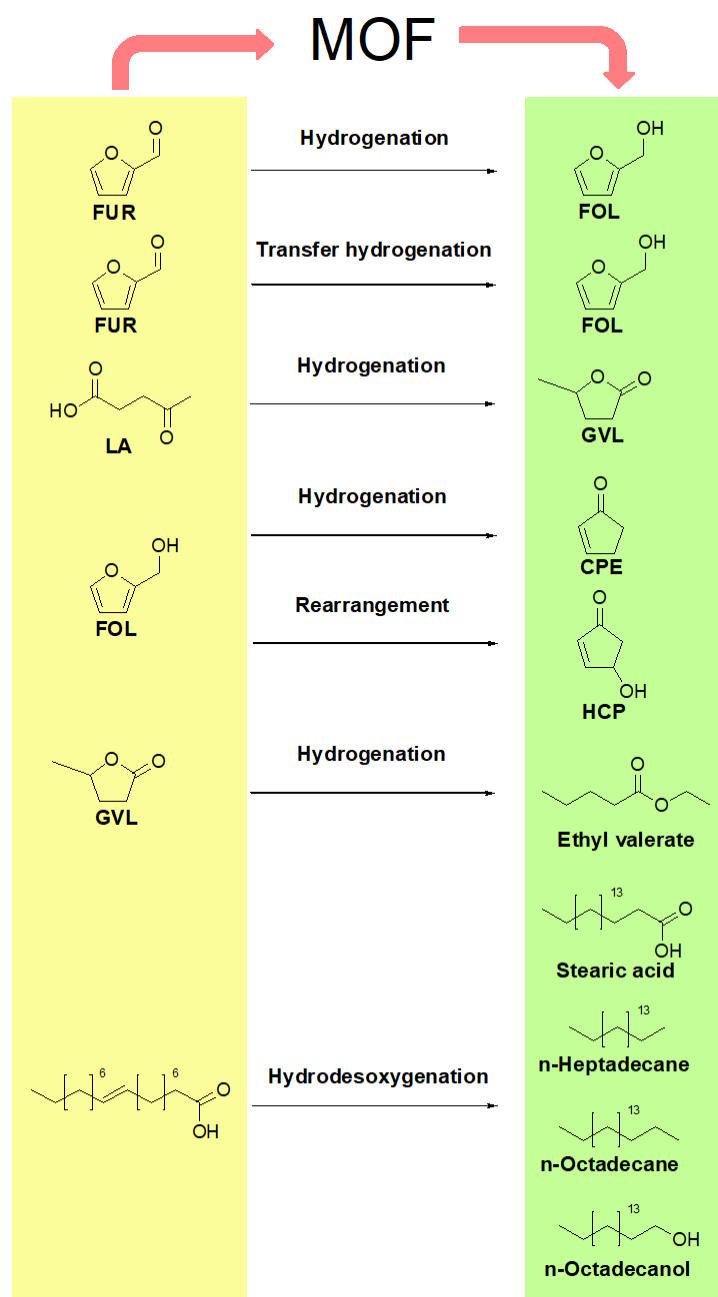


**Figure 4.** Main products starting from different biomass precursors.

### 3.2. Oxidation

#### MOFs as Sacrifice Templates (MOF Derived Catalysts)

As already mentioned, the use of MOFs as heterogeneous catalysts is based on the adequate structural properties of the material, such as the ordered metal ions distribution and the porosity of the MOF, which allows a good substrate diffusion in the catalytic process [91–93]. However, the use of MOFs as sacrifice templates to obtain metal nanoparticles (NPs) or supported metal oxides has become of great interest [94–96]. This method usually consists of the generation of a MOF-support or MOF-nanoparticle system, which is then calcinated or pyrolyzed [97], yielding a material with the reduced metal ions from the MOF highly dispersed along the support or as nanoparticles. This allows the combination of the porous properties of the support with the ordered dispersion of the catalytically active species, producing a metal-support interface with interesting properties.

Yu-Te Liao et al. [98] reported the preparation of the cage shaped catalysts,  $Au_xPd@Co_3O_4$ , used in the oxidation of 5-hydroxymethylfurfural (HMF). These materials are alloys of Au-Pd nanoparticles supported on cobalt oxide and were obtained using a De novo process, reported previously by the same group [99,100]. This method mixes gold and palladium ions with the linkers and Co ions before producing ZIF-67. This yields the Au-Pd-ZIF-67 system, which is then calcinated to form the  $Au_xPd@Co_3O_4$  catalysts.

The catalysts were prepared with different Au/Pd ratios, i.e., 0.1:0, 0.1:0.1, 0.05:0.1, 0.1:0.2, 0.05:0.2, 0.025:0.2, 0:0.2. The surface area and the pore size varied from 11 to  $75\text{ m}^2\text{ g}^{-1}$  and 10 to 55 nm, respectively. The highest performing catalyst,  $Au_{0.5}Pd@Co_3O_4$  (Au/Pd ratio 0.1:0.1), presents a specific surface area of  $64\text{ m}^2\text{ g}^{-1}$ , much lower than the original MOF specific surface area,  $722\text{ m}^2\text{ g}^{-1}$ , due to the decomposition of the organic framework. Even when it is known that a high specific surface area enhances the catalytic activity of a MOF [97], in this case, the original structure is sacrificed to prioritize a better interaction with  $Co^{II}$  ions. The thermal treatment performed on the precursor (Au-Pd-ZIF-67) is relevant, because this method allows a uniform distribution of the metallic NPs in the  $Co_3O_4$  cages, corroborated by TEM-EDX. Moreover, XPS analysis confirmed the presence of highly active  $Au^I$  ions in the interface between the NPs alloy and the  $Co_3O_4$  support. The  $Au^I$  ion formation has been observed in systems where Au is embedded within reducible oxide supports [101,102]. To clarify the contribution of the MOF synthesis method upon the presence of  $Au^I$  ions, the authors compared  $Au_{0.5}Pd/Co_3O_4$ , obtained with the Sol-immobilization method, with  $Au_{0.5}Pd@Co_3O_4$ , obtained with the De novo method, showing  $Au^+/Au^0$  ratios of 0 and 0.23, respectively. This study served to verify that the method used to synthesize the MOF affects the presence of  $Au^I$  ions. In the De novo method, the metallic NPs are surrounded by the ZIF-67 crystalline lattice that contains uniformly distributed  $Co^{II}$  ions, while in the Sol-immobilization method, the NPs are attached to the  $Co_3O_4$  affecting the interface between the Au and the  $Co_3O_4$ . This was also proved by the  $Co^{III}/Co^{II}$  ratio in the cages of  $Au_{0.5}Pd/Co_3O_4$  y  $Au_{0.5}Pd@Co_3O_4$  (2.52 and 2.13, respectively), showing that there is a higher interaction between the metallic NPs and the  $Co_3O_4$  in the  $Au_{0.5}Pd@Co_3O_4$  system. A lower  $Co^{III}/Co^{II}$  ratio represents a higher interaction because it has been demonstrated that  $Au^0$  and/or  $Pd^0$  interact with  $Co^{III}$ , forming  $Au^{+\delta}$ ,  $Pd^{II}$  y  $Co^{II}$  ions and decreasing the  $Co^{III}/Co^{II}$  ratio [103].

The catalytic results indicate that  $Au_xPd@Co_3O_4$  catalysts present rather high HMF conversion values (from 57% to 100%) to different products, i.e., 5-hydroxymethyl-2-furancarboxylic acid (HMFA), 2,5-diformylfuran (DFF), 5-formylfurancarboxylic acid (FFCA) and 2,5-furandicarboxylic acid (FDCA). The best results were achieved with the  $Au_{0.5}Pd@Co_3O_4$ , which presented a 100% conversion and 95% selectivity towards the desired product FDCA at 90 °C, using NaOH and  $Na_2CO_3$  as basic media and 10%  $H_2O_2$  as the oxidizing agent. The good results are attributed to the cage-like structure of  $Au_{0.5}Pd@Co_3O_4$  that has a homogeneous distribution of the Au-Pd NPs covered by the cobalt ions, thus increasing the Au/ $Co_3O_4$  interface. These structural features are necessary for the catalytic process to occur since Pd forms part of the NPs alloy, allowing an increase of  $Au^I$  ions. The presence of Au and  $Au^I$  ions produces hemiacetal and alcoxide intermediates in the catalytic process, which then interact with hydroperoxide radicals and oxygen produced in situ along the Au- $Co_3O_4$  interface. This allows the generation of HMFA, FFCA and FDCA [101,104,105]. The high performance of  $Au_{0.5}Pd@Co_3O_4$  in the oxidation of HMF to FDCA is mainly attributed to the Au- $Co_3O_4$  interface that facilitates the HMFA oxidation to FFCA. This is a slow step in the reaction, and it is relevant in the production of FDCA [106,107]. On the other hand, there is an important contribution from the hydroperoxide radicals produced from the  $H_2O_2$ , which activates the Lewis acid sites on the  $Co_3O_4$  and  $Au^I$  and accelerates the oxidation reaction.

Feng et al. [108] also used ZIF-67 as a sacrifice template to obtain cobalt-based N-doped carbon materials (Co@C-N), using these as heterogeneous catalysts in the oxidative esterification of HMF to produce dimethyl furandicarboxylic acid (DMFDCA). Unlike the work of Yu-Te Liao et al., this group pyrolyzed ZIF-67 alone to generate Co@C-N

derivatives. The thermogravimetric analysis determined the pyrolysis temperature; this is when the organic linkers decompose over 500 °C. Thus, pyrolysis temperatures of 600, 700, 800 and 900 °C were used. It was determined that the transformation of ZIF-67 into metallic Co implies a mass loss of 73.3%. However, for this system, the mass loss for the temperatures mentioned previously was between 28.3% and 46.6%. This indicates the formation of a carbon-containing material instead of a material composed of only Co NPs. To better understand the structural aspects of the catalysts, XRD analyses were performed on the Co@C–N materials. The results showed the presence of graphite carbon sheets and metallic Co. The intensity of the diffraction peaks suggests the formation of a Co phase with a high crystallization degree. On the other hand, the Raman spectra of the Co@C–N samples revealed G and D carbon bands characteristic for sp<sup>2</sup> graphite carbon and disoriented carbon, respectively [109]. The intensity ratio of the I<sup>G</sup>/I<sup>D</sup> bands for the Co@C–N (600), Co@C–N (700), Co@C–N (800) and Co@C–N (900) materials was 0.86, 0.97, 1.29 and 1.97, respectively, which reveals that the crystalline degree of graphite carbon could be improved with higher temperatures. These results make clear that it is possible to obtain carbon-based materials containing Co NPs.

As mentioned above, the thermal treatment used on the MOF precursor is key to achieving an adequate distribution of metallic NPs over the material structure, since it derives in good dispersion of the catalytically active sites. SEM analysis proved that this was achieved since the pyrolyzed NPs roughly kept the polyhedral form of ZIF-67 with a slight contraction. Moreover, the SEM analysis made evident that the Co NPs were highly dispersed on the material, which was mainly due to the order of the organic linkers from the ZIF-67 precursor.

The presence of nitrogen and its influence in the catalytic process was investigated as well. The N content for Co@C–N (600), Co@C–N (700), Co@C–N (800) y Co@C–N (900) was found to be 9.7, 5.8, 2.1 and 0.6%, respectively, showing a decrease at higher temperatures. Besides, two kinds of nitrogen species were found by XPS technique in the Co@C–N catalysts by two high-resolution N1s peaks that suggest the presence of pyridine nitrogen (c.a. 399 eV) and graphite nitrogen (c.a. 401 eV) [110]. These results indicate that the relative content of graphite N increased with the pyrolysis temperature, while the relative pyridine N content decreased as the used temperature was increased. This implies a higher graphitization at higher temperatures, which is beneficial for better electronic mobility. Reports indicate that a strong interaction between metallic NPs and graphite walls can enhance the activity of nanocarbon catalysts' activity due to the electron transfer from the metal atoms to the carbon shells; a process that occurs until the Fermi level reaches equilibrium [111,112]. Moreover, the pyridine N doping produces structural flaws in the C–N compounds when forming the O<sub>2</sub> adsorption sites and basic sites, which are necessary for the formation of oxygen radicals, as well as the substrate interaction with the surface of the catalysts. These structural features had a clear repercussion in the catalytic results obtained for the oxidative esterification of HMF to produce DMFDCA.

The catalytic reactions were performed at 100 °C, using sodium carbonate as the base, methanol as the solvent and 2 MPa of molecular oxygen as the oxidant. The most active catalyst turned out to be Co@C–N (800) since it showed an appropriate nitrogen content in its structure and a relatively high graphitic-N/C ratio, which contributed to the balance between the nitrogen contents and nitrogen species. This balance can result in higher electron mobility and more active sites, which helps in the activation and reduction of O<sub>2</sub>. The strong electronic interaction between the Co atoms and N-doping carbon is prone to generate strong electron acceptors (Co nanoparticles) and electron donors (C–N composites), leading to the high catalytic activity of Co@C–N (800) in the oxidative esterification reaction.

Another example of a MOF as a sacrifice template was reported by Bao et al. [113] who synthesized an active catalyst for the aerobic oxidation of HMF to FDCA with holey 2D Mn<sub>2</sub>O<sub>3</sub> nanoflakes (M400). These were obtained by the calcination of the MnTPA-MOF at 400 °C. A remarkable detail is that the thermal treatment used on the MnTPA precursor

generates a change in the MOF structure. This was observed in the calcination at 250, 300, 350 and 400 °C of MnTPA to obtain the M250, M300, M350 and M400 materials, respectively. The PXRD, FESEM and N<sub>2</sub> adsorption/desorption characterization analysis demonstrated these structural changes caused by the used calcination temperature. The PXRD diffractograms showed that the thermal treatment at 250 and 300 °C (M250 and M300) resulted in the decreasing and widening of the diffraction peaks compared to the MnTPA precursor, which implies the solvent elimination and partial amorphization of the original MOF. When the temperature rises to 350 °C, the diffraction peaks of the MnTPA precursor completely disappear, generating peaks that can be attributed to Mn<sub>2</sub>O<sub>3</sub> (JCPDS 41-1442) and Mn<sub>3</sub>O<sub>4</sub> (JCPDS 01-1127). This suggests the decomposition of the crystalline MnTPA, forming metal oxides. The data collected from the FESEM analysis supports this theory as a flake-like structure is observed with a smooth surface and a thickness of 60–130 nm for the pristine MnTPA, which is preserved in the M250 and M300 material with few differences in surface and thickness. For the M350 material, the surface of the flakes became rough, and pores began to appear as the thickness decreased to 30 nm. When the calcination temperature increased to 400 °C, the thickness of the flakes was ca. 20 nm, and more holes were observed. This, combined with the FTIR spectra of all materials, showed that the structure changes due to the decomposition of the organic linkers losing the crystalline structure to yield metal oxides. It is worth mentioning that the morphological changes aim for a higher surface area of the catalyst, which, as we have seen before, is a very important factor for the catalytic activity of any heterogeneous catalyst. N<sub>2</sub> adsorption/desorption studies were performed, and the results corroborate a higher porosity of M400 over the rest of the materials. The study showed that M400 presents a surface area of 61.5 m<sup>2</sup> g<sup>-1</sup> while the pore size distribution showed micropores of 2.4 nm and mesopores of 22.7 nm, attributed to the nanoflakes pores and the interflake pores, respectively, proving that the M400 material presented the most adequate characteristics to be used as the catalyst.

Another important characteristic in a catalyst is the presence of metallic species that have an adequate redox couple to carry out the catalytic process. XPS spectra showed that M400 presented Mn<sup>II</sup>, Mn<sup>III</sup> and Mn<sup>IV</sup> ions, which allowed the presence of Mn<sup>II</sup>/Mn<sup>IV</sup> and Mn<sup>III</sup>/Mn<sup>IV</sup> redox couples (peak intensities of 0.36 and 0.77, respectively). These data indicate a relatively high proportion of Mn<sup>IV</sup> with respect to the other oxidation states.

M350 and M400 were selected as catalysts for the aerobic oxidation of HMF to FDCA due to the structural properties of these materials. The reactions were made at 100 °C and 1.4 Mpa of O<sub>2</sub> in the presence of NaHCO<sub>3</sub> (three equivalents of NaHCO<sub>3</sub> for each equivalent of HMF) for 24 h. For comparison, the same reaction conditions were used in three other reactions, i.e., in the absence of the catalyst, using activated Mn<sub>2</sub>O<sub>3</sub> as the catalyst and using activated MnO<sub>2</sub> as the catalyst. The results showed that in the absence of any catalyst, the total yield of HMFCFA and FDCA was below 4%. For the activated Mn<sub>2</sub>O<sub>3</sub>, the total yield for HMFCFA, FFCA and FDCA did not surpass 13%, and for the activated MnO<sub>2</sub>, only a 12% yield was observed for the desired FDCA, with a 91.1% of HMF conversion, revealing a poor selectivity. The M350 material showed an almost total HMF conversion with an FDCA total yield of 76.1%, but this was lower than the 99.5% FDCA yield of M400 with a 100% HMF conversion. This difference was attributed to the presence of Mn<sub>3</sub>O<sub>4</sub> in the M350 structure, while the good results obtained with M400 as the catalyst were attributed to the abundant surface pores present in the M400 material since they allow a better substrate diffusion and increased the catalytically active sites available on the catalyst surface.

Up to this point, it has become evident that the pyrolysis temperature is important to obtain a heterogeneous catalyst with adequate structural properties such as pore size, surface area, metal dispersion and metal-support interface. Fang et al. [114] remark on the importance of thermal control in the synthesis process. In this work, the ZIF-67 MOF was encapsulated in the mesoporous silica KIT-6, which acted as support to obtain the ZIF-67@KIT-6 precursor. This precursor was then calcinated at 250 °C to produce a catalyst

with highly dispersed cobalt oxide NPs that maintained the support structure (Co@KIT-6). The authors indicated that the control of certain parameters, such as heating rate, temperature and calcination time, was crucial to achieving ultrafine metal oxide NPs. In this work, a sufficient calcination time was critical for the complete oxidation of metal ions and the elimination of organic linkers. The calcination temperature and the heating rate were carefully set to 250 °C (above the MOF decomposition temperature in an O<sub>2</sub> atmosphere [115]) and 1 °C/min respectively. According to the Kirkendall effect, the dispersed and ordered metal ions tend to aggregate to reduce their surface-free energy under thermal treatment. At higher temperatures (e.g., 275 °C or 300 °C), the metal ions are more prone to aggregate in bigger particles (>5 nm). On the other hand, faster heating rates (2 and 3 °C/min) accelerate the decomposition process, producing larger aggregates (c.a. 5 nm). Hence, the key elements to achieve ultrafine Co<sub>3</sub>O<sub>4</sub> NPs were slow heating rates, low calcination temperatures and sufficient thermolysis time.

Co@KIT-6 was used as a catalyst in the aerobic oxidation of HMF to obtain FDCA at 80 °C while using water as solvent. The authors made a comparative study using KIT-6 and Co/KIT-6. The original KIT-6 did not present conversion under the reaction conditions. Besides, the Co/KIT-6 prepared with a typical impregnation method exhibited a poor activity, achieving a 10% HMF conversion and total FDCA yield of 9.5%. The results obtained with Co@KIT-6 indicated a 100% HMF conversion with a 99% selectivity towards the desired FDCA. These good results were attributed to the presence of highly oxidant ultrafine Co<sub>3</sub>O<sub>4</sub> NPs confined in the KIT-6 mesopores, which were effective for the oxidation of HMF to FDCA, following the Mars van Krevelen reaction mechanism. According to this mechanism, the lattice oxygen in Co<sub>3</sub>O<sub>4</sub> facilitates HMF oxidation to FDCA, being subsequently replenished by the oxygen present in the reaction atmosphere.

Fang et al. [116] have also reported the synthesis of FeCo/C bimetallic catalysts, used in the aerobic oxidation reaction of HMF to obtain DFF. In this case, the FeCo/C catalysts were obtained from MIL-45b MOF by thermolysis at 500, 600, 700 and 800 °C, with a heating rate of 1 °C min<sup>-1</sup> for 6 h. These were named FeCo/C(T), where T represents the calcination temperature. The studies indicate that the best catalyst was FeCo/C(500), with which conversion and selectivity of >99% to the DFF product were obtained. The good results were attributed to the fact that the hollow structure of the FeCo/C(500) catalyst promotes the adsorption of HMF, as well as the rapid desorption of the formed DFF, leading to a higher product yield. The catalysts obtained at higher temperatures, i.e., 600, 700 and 800, did not present the same properties since the pores collapsed due to the effect of the temperature. This highlights that thermal control in the synthesis of the catalyst is a relevant parameter. The summary of the reactions and its catalytic results are shown in the Figure 5 and Table 4.

**Table 4.** Catalytic conditions for the different catalysts of Figure 5 in the HMF oxidation.

	Catalyst (mg)	Substrate (mmol)	Base	Oxidant	Temperature (°C)	Time (h)	Conv. HMF (%)	Ref.
a	10	0.3	NaOH	H <sub>2</sub> O <sub>2</sub>	90	1	100	[98]
b	10	0.3	NaOH/Na <sub>2</sub> CO <sub>3</sub>	H <sub>2</sub> O <sub>2</sub>	90	1	100	[98]
c	100	0.5	Na <sub>2</sub> CO <sub>3</sub>	O <sub>2</sub>	100	5	99	[108]
d	100	0.5	Na <sub>2</sub> CO <sub>3</sub>	O <sub>2</sub>	100	5	99	[108]
e	150	50 mM	NaHCO <sub>3</sub>	O <sub>2</sub>	100	24	>99	[113]
f	150	50 mM	NaHCO <sub>3</sub>	O <sub>2</sub>	100	24	>99	[113]
g	1 mol%	0.1	-	Air	80	2	100	[114]
h	20 mol%	1	Na <sub>2</sub> CO <sub>3</sub>	O <sub>2</sub>	100 °C	6	>99	[116]

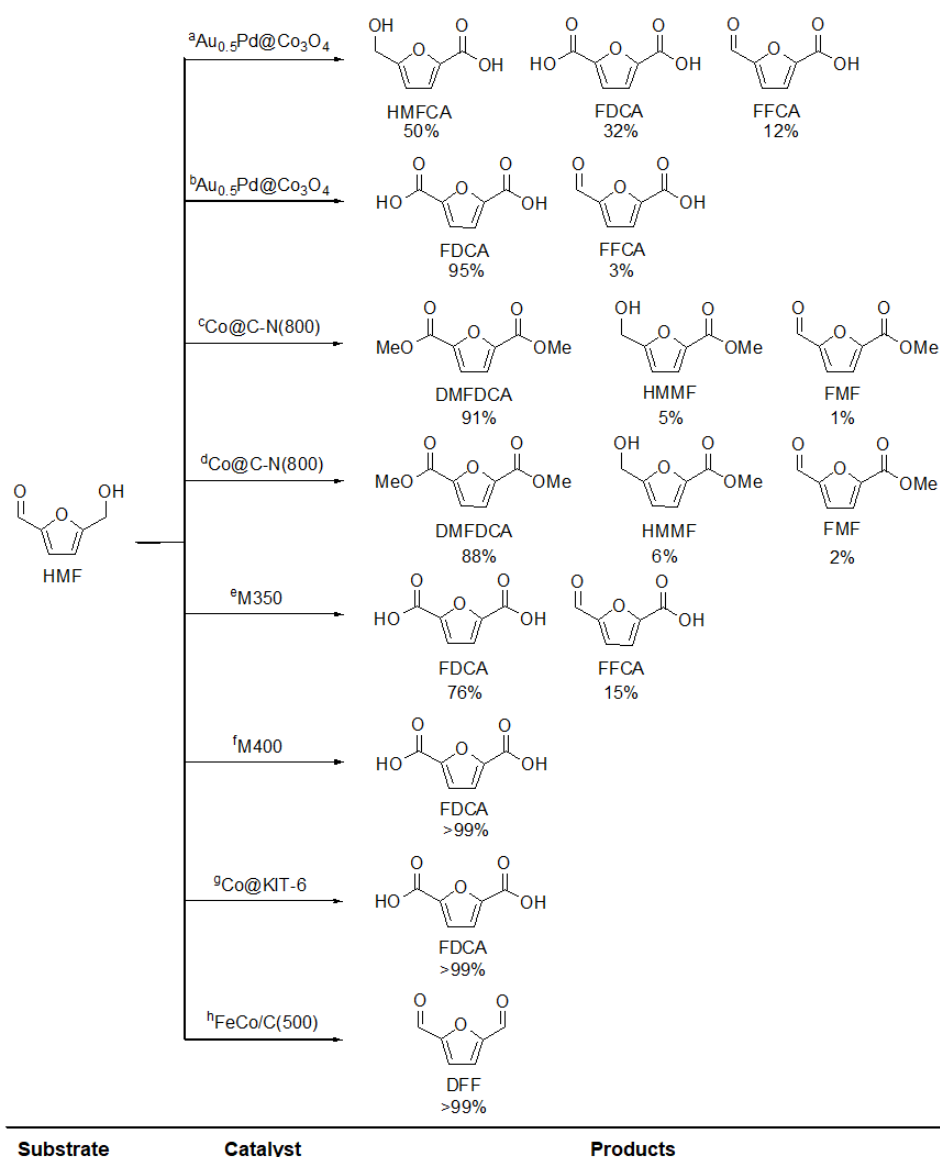


**Figure 5.** HMF oxidation with different catalysts, synthesized using MOFs as sacrifice templates.

### 3.3. Perspectives and Conclusions

It is evident that MOFs are a great alternative to be used in the synthesis of heterogeneous catalysts due to their high number of properties and versatility. Due to this, it is important that this type of compound be studied in catalytic reactions that involve the use of substrates from biomass. In this way, the properties of MOFs that were described in this section are necessary to achieve good results in chemical transformations, which involve platform compounds such as furfural or levulinic acid, since their derivatives are important in the current chemical industry.

In this chapter, four properties were highlighted that are considered relevant when designing a heterogeneous catalyst—based on MOFs for hydrogenation reactions—and that can finally be extrapolated to other catalytic reactions. The first important characteristics are the pore size and the dispersion of the nanoparticles within the MOF. Both are important because they are related to the accessibility of the substrate to the active sites of the catalyst, and the availability of these sites to carry out the catalytic process. In both cases, the choice of the MOF and the catalyst synthesis method are important. Second, the type of acidic sites that the catalyst may have must be considered, these being the Brönsted and Lewis acidic sites. The acidic sites are essential to generate the possibilities of interaction of the substrate with the active metallic sites of the catalyst; in addition, being able to modulate

the selectivity of the reaction, depending on the type of acid site. Finally, the connectivity of the metallic nodes with the ligands must be taken into account in such a way that there is an optimal ratio of connected nodes that allows maintaining an adequate pore size and high availability of active acid sites. It is possible to note that all the aforementioned characteristics point to two central properties, the availability of the active sites of the catalyst and the accessibility of the substrate to these active sites. Therefore, we consider these parameters and the relationship between them to be of vital importance in designing MOFs that may have interesting potential in the transformation of biomass.

**Funding:** This research was funded by PROYECTO FONDECYT INICIACION 1119042.

**Data Availability Statement:** Not applicable.

**Conflicts of Interest:** The authors declare no conflict of interest.

## References

1. Yu, D.; He, L. Introduction to CO<sub>2</sub> utilization. *Green Chem.* **2021**, *23*, 3499–3501. [[CrossRef](#)]
2. Garba, M.; Usman, M.; Khan, S. CO<sub>2</sub> towards fuels: A review of catalytic conversion of carbon dioxide to hydrocarbons. *J. Environ. Chem. Eng.* **2021**, *9*, 104756. [[CrossRef](#)]
3. Chen, Z.; Du, S.; Zhang, J.; Wu, X. From ‘Giff’ to gift: Producing organic solvents from CO<sub>2</sub>. *Green Chem.* **2020**, *22*, 8169–8182. [[CrossRef](#)]
4. Hwang, S.-M.; Zhang, C.; Han, J.H.; Park, H.-G.; Kim, Y.T.; Yang, S.; Jun, K.-W.; Kim, S.K. Mesoporous carbon as an effective support for Fe catalyst for CO<sub>2</sub> hydrogenation to liquid hydrocarbons. *J. CO<sub>2</sub> Util.* **2020**, *37*, 65–73. [[CrossRef](#)]
5. Wang, J.; Al Qahtani, M.; Wang, X. One-step plasma-enabled catalytic carbon dioxide hydrogenation to higher hydrocarbons: Significance of catalyst-bed configuration. *Green Chem.* **2021**, *23*, 1642–1647. [[CrossRef](#)]
6. Wang, Y.; Winter, L.; Chen, J.; Yan, B. CO<sub>2</sub> hydrogenation over heterogeneous catalysts at atmospheric pressure: From electronic properties to product selectivity. *Green Chem.* **2021**, *23*, 249–267. [[CrossRef](#)]
7. Li, X.; Luo, X.; Jin, Y. Heterogeneous sulfur-free hydrodeoxygenation catalysts for selectively upgrading the renewable bio-oils to second generation biofuels. *Renew. Sustain. Energy Rev.* **2018**, *82*, 3762–3797. [[CrossRef](#)]
8. Santillan-Jimenez, E.; Crocker, M. Catalytic deoxygenation of fatty acids and their derivatives to hydrocarbon fuels via decarboxylation/decarbonylation. *J. Chem. Technol. Biotechnol.* **2012**, *87*, 1041–1050. [[CrossRef](#)]
9. Davis, K.; Yoo, S.; Shuler, E.; Sherman, B.; Lee, S.; Leem, G. Photocatalytic hydrogen evolution from biomass conversion. *Nano Converg.* **2021**, *8*, 6. [[CrossRef](#)]
10. Rajeswari, G.; Jacob, S.; Chandel, A.; Kumar, V. Unlocking the potential of insect and ruminant host symbionts for recycling of lignocellulosic carbon with a biorefinery approach: A review. *Microb. Cell. Fact* **2021**, *20*, 107. [[CrossRef](#)]
11. Serrano-Ruiz, J.C.; West, R.M.; Dumesic, J.A. Catalytic Conversion of Renewable Biomass Resources to Fuels and Chemicals. *Annu. Rev. Chem. Biomelecular Eng.* **2010**, *1*, 79–100. [[CrossRef](#)] [[PubMed](#)]
12. Rodríguez-Padrón, D.; Zhao, D.; Carrillo-Carrion, C. Exploring the potential of biomass-templated Nb/ZnO nanocatalysts for the sustainable synthesis of N-heterocycles. *Catal. Today* **2021**, *368*, 243–249. [[CrossRef](#)]
13. Galarza, E.; Fermanelli, C.; Pierella, L.; Saux, C.; Renzini, M. Influence of the Sn incorporation method in ZSM-11 zeolites in the distribution of bio-oil products obtained from biomass pyrolysis. *J. Anal. Appl. Pyrolysis* **2021**, *156*, 105116. [[CrossRef](#)]
14. Liang, J.; Shan, G.; Sun, Y. Catalytic fast pyrolysis of lignocellulosic biomass: Critical role of zeolite catalysts. *Renew. Sustain. Energy Rev.* **2021**, *139*, 110707. [[CrossRef](#)]
15. Ribeiro, L.; de Melo Órfão, J.; Ribeiro Pereira, M. An overview of the hydrolytic hydrogenation of lignocellulosic biomass using carbon-supported metal catalysts. *Mater. Today Sustain.* **2020**, *11*, 100058. [[CrossRef](#)]
16. Safaei, M.; Foroughi, M.; Ebrahimpour, N.; Jahani, S.; Omid, A.; Khatami, M. A review on metal–organic frameworks: Synthesis and applications. *TrAC Trends Anal. Chem.* **2019**, *118*, 401–425. [[CrossRef](#)]
17. Zhang, L.; Li, S.; Xin, J. A non-enzymatic voltammetric xanthine sensor based on the use of platinum nanoparticles loaded with a metal–organic framework of type MIL-101(Cr). Application to simultaneous detection of dopamine, uric acid, xanthine and hypoxanthine. *Microchim. Acta* **2019**, *186*. [[CrossRef](#)]
18. Mirkovic, I.; Lei, L.; Ljubic, D.; Zhu, S. Crystal Growth of Mmetal-Organic Framework-5 around Cellulose-Based Fibers Having a Necklace Morphology. *ACS Omega* **2019**, *4*, 169–175. [[CrossRef](#)]
19. Zhang, L.; Jiang, K.; Zhang, J. Low-Cost and High-Performance Microporous Mmetal-Organic Framework for Separation of Acetylene from Carbon Dioxide. *ACS Sustain. Chem. Eng.* **2018**, *7*, 1667–1672. [[CrossRef](#)]
20. Huan, W.; Xing, M.; Cheng, C.; Li, J. Facile Fabrication of Magnetic Mmetal-Organic Framework Nanofibers for Specific Capture of Phosphorylated Peptides. *ACS Sustain. Chem. Eng.* **2018**, *7*, 2245–2254. [[CrossRef](#)]
21. Wei, X.; Wang, Y.; Chen, J. Poly(deep eutectic solvent)-functionalized magnetic metal organic framework composites coupled with solid-phase extraction for the selective separation of cationic dyes. *Anal. Chim. Acta* **2019**, *1056*, 47–61. [[CrossRef](#)] [[PubMed](#)]

22. Yi, X.; He, X.; Yin, F.; Chen, B.; Li, G.; Yin, H. Co-CoO-Co<sub>3</sub>O<sub>4</sub>/N-doped carbon derived from metal organic framework: The addition of carbon black for boosting oxygen electrocatalysis and Zn-Air battery. *Electrochim. Acta* **2019**, *295*, 966–977. [[CrossRef](#)]
23. Cao, A.; Zhang, L.; Wang, Y. 2D–2D Heterostructured UNiMOF/g-C<sub>3</sub>N<sub>4</sub> for Enhanced Photocatalytic H<sub>2</sub> Production under Visible-Light Irradiation. *ACS Sustain. Chem. Eng.* **2018**, *7*, 2492–2499. [[CrossRef](#)]
24. Baek, J.; Rungtaweeworant, B.; Pei, X. Bioinspired Metal-Organic Framework Catalysts for Selective Methane Oxidation to Methanol. *J. Am. Chem. Soc.* **2018**, *140*, 18208–18216. [[CrossRef](#)] [[PubMed](#)]
25. Andrew, R.M. Global CO<sub>2</sub> emissions from cement production. *Earth Syst. Sci. Data Discuss.* **2018**, *10*, 195–217. [[CrossRef](#)]
26. Aresta, M. Carbon dioxide reduction to C<sub>1</sub> or C<sub>n</sub> molecules. In *Carbon Dioxide Recovery and Utilization*; Aresta, M., Ed.; Springer: Dordrecht, The Netherlands, 2003; pp. 293–312.
27. Whang, H.S.; Lim, J.; Choi, M.S.; Lee, J.; Lee, H. Heterogeneous catalysts for catalytic CO<sub>2</sub> conversion into value-added chemicals. *BMC Chem. Eng.* **2019**, *1*, 9. [[CrossRef](#)]
28. Wei, J.; Ge, Q.; Yao, R.; Wen, Z.; Fang, C.; Guo, L.; Xu, H.; Sun, J. Directly converting CO<sub>2</sub> into a gasoline fuel. *Nat. Commun.* **2017**, *8*, 15174. [[CrossRef](#)]
29. Porosoff, M.D.; Yan, B.; Chen, J.G. Catalytic reduction of CO<sub>2</sub> by H<sub>2</sub> for synthesis of CO, methanol and hydrocarbons: Challenges and opportunities. *Energy Environ. Sci.* **2016**, *9*, 62–73. [[CrossRef](#)]
30. Li, W.; Wang, H.; Jiang, X.; Zhu, J.; Liu, Z.; Guo, X.; Song, C. A short review of recent advances in CO<sub>2</sub> hydrogenation to hydrocarbons over heterogeneous catalysts. *RSC Adv.* **2018**, *8*, 7651–7669. [[CrossRef](#)]
31. Gao, P.; Dang, S.; Li, S.; Bu, X.; Liu, Z.; Qiu, M.; Yang, C.; Wang, H.; Zhong, L.; Han, Y.; et al. Direct production of lower olefins from CO<sub>2</sub> conversion via bifunctional catalysis. *ACS Catal.* **2018**, *8*, 571–578. [[CrossRef](#)]
32. Fujiwara, M.; Ando, H.; Tanaka, M.; Souma, Y. Hydrogenation of carbon dioxide over Cu Zn-chromate/zeolite composite catalyst: The effects of reaction behavior of alkenes on hydrocarbon synthesis. *Appl. Catal. A Gen.* **1995**, *130*, 105–116. [[CrossRef](#)]
33. Dang, S.; Gao, P.; Liu, Z.; Chen, X.; Yang, C.; Wang, H.; Zhong, L.; Li, S.; Sun, Y. Role of zirconium in direct CO<sub>2</sub> hydrogenation to lower olefins on oxide/zeolite bifunctional catalysts. *J. Catal.* **2018**, *364*, 382–393. [[CrossRef](#)]
34. Gao, J.; Jia, C.; Liu, B. Direct and selective hydrogenation of CO<sub>2</sub> to ethylene and propene by bifunctional catalysts. *Catal. Sci. Technol.* **2017**, *7*, 5602–5607. [[CrossRef](#)]
35. Fujiwara, M.; Kieffer, R.; Ando, H.; Xu, Q.; Souma, Y. Change of catalytic properties of FeZnO/zeolite composite catalyst in the hydrogenation of carbon dioxide. *Appl. Catal. A Gen.* **1997**, *154*, 87–101. [[CrossRef](#)]
36. Helal, A.; Usman, M.; Arafat, M.E.; Abdelnaby, M.M. Alkyl functionalized UiO-66 metal-organic framework as a catalyst for the synthesis of cyclic carbonates by CO<sub>2</sub> cycloaddition. *J. Ind. Eng. Chem.* **2020**, *89*, 104–110. [[CrossRef](#)]
37. Helal, A.; Cordova, K.E.; Arafat, M.E.; Usman, M.; Yamani, Z.H. Defect-engineering a metal-organic framework for CO<sub>2</sub> fixation in the synthesis of bioactive oxazolidinones. *Inorg. Chem. Front.* **2020**, *7*, 3571–3577. [[CrossRef](#)]
38. Santibañez, L.; Escalona, N.; Torres, J.; Kremer, C.; Cancino, P.; Spodine, E. Cu<sup>II</sup>- and Co<sup>II</sup>-Based MOFs: {[La<sub>2</sub>Cu<sub>3</sub>(μ-H<sub>2</sub>O)(ODA)<sub>6</sub>(H<sub>2</sub>O)<sub>3</sub>·3H<sub>2</sub>O]<sub>n</sub> and {[La<sub>2</sub>Co<sub>3</sub>(ODA)<sub>6</sub>(H<sub>2</sub>O)<sub>6</sub>·12H<sub>2</sub>O]<sub>n</sub>. The Relevance of Physicochemical Properties on the Catalytic Aerobic Oxidation of Cyclohexene. *Catalysts* **2020**, *10*, 589. [[CrossRef](#)]
39. Cancino, P.; Santibañez, L.; Stevens, C.; Fuentealba, P.; Audebrand, N.; Aravena, D.; Torres, J.; Martinez, S.; Kremer, C.; Spodine, E. Influence of the channel size of isostructural 3d–4f MOFs on the catalytic aerobic oxidation of cycloalkenes. *New J. Chem.* **2019**, *43*, 11057–11064. [[CrossRef](#)]
40. Han, Y.; Xu, H.; Su, Y.; Xu, Z.-l.; Wang, K.; Wang, W. Noble metal (Pt, Au@Pd) nanoparticles supported on metal organic framework (MOF-74) nanoshuttles as high-selectivity CO<sub>2</sub> conversion catalysts. *J. Catal.* **2019**, *370*, 70–78. [[CrossRef](#)]
41. Wang, T.; Shi, L.; Tang, J.; Malgras, V.; Asahina, S.; Liu, G.; Zhang, H.; Meng, X.; Chang, K.; He, J.; et al. A Co<sub>3</sub>O<sub>4</sub>-embedded porous ZnO rhombic dodecahedron prepared using zeolitic imidazolate frameworks as precursors for CO<sub>2</sub> photoreduction. *Nanoscale* **2016**, *8*, 6712–6720. [[CrossRef](#)]
42. Zhang, H.; Wang, T.; Wang, J.; Liu, H.D.; Dao, T.; Li, M.; Liu, G.; Meng, X.; Chang, K.; Shi, L.; et al. Surface-Plasmon-Enhanced Photodriven CO<sub>2</sub> Reduction Catalyzed by Metal-Organic-Framework-Derived Iron Nanoparticles Encapsulated by Ultrathin Carbon Layers. *Adv. Mater.* **2016**, *28*, 3703–3710. [[CrossRef](#)] [[PubMed](#)]
43. Wang, S.; Guan, B.Y.; Lu, Y.; Lou, X.W.D. Formation of Hierarchical In<sub>2</sub>S<sub>3</sub>–CdIn<sub>2</sub>S<sub>4</sub> Heterostructured Nanotubes for Efficient and Stable Visible Light CO<sub>2</sub> Reduction. *J. Am. Chem. Soc.* **2017**, *139*, 17305–17308. [[CrossRef](#)] [[PubMed](#)]
44. Hu, S.; Liu, M.; Ding, F.; Song, C.; Zhang, G.; Guo, X. Hydrothermally stable MOFs for CO<sub>2</sub> hydrogenation over iron-based catalyst to light olefins. *J. CO<sub>2</sub> Util.* **2016**, *15*, 89–95. [[CrossRef](#)]
45. Tarasov, A.L.; Isaeva, V.I.; Tkachenko, O.P.; Chernyshev, V.V.; Kustov, L.M. Conversion of CO<sub>2</sub> into liquid hydrocarbons in the presence of a Co-containing catalyst based on the microporous metal-organic framework MIL-53(Al). *Proc. Tech.* **2018**, *176*, 101–106. [[CrossRef](#)]
46. Zhao, Z.-W.; Zhou, X.; Liu, Y.-N.; Shen, C.-C.; Yuan, C.-Z.; Jiang, Y.-F.; Zhao, S.-J.; Ma, L.-B.; Cheang, T.-Y.; Xu, A.-W. Ultrasmall Ni nanoparticles embedded in Zr-based MOFs provide high selectivity for CO<sub>2</sub> hydrogenation to methane at low temperatures. *Catal. Sci. Technol.* **2018**, *8*, 3160–3165. [[CrossRef](#)]
47. Zhen, W.; Gao, F.; Tian, B.; Ding, B.; Deng, Y.; Li, Z.; Gao, H.; Lu, G. Enhancing activity for carbon dioxide methanation by encapsulating (111) facet Ni particle in metal-organic frameworks at low temperature. *J. Catal.* **2017**, *348*, 200–211. [[CrossRef](#)]
48. Zhen, W.; Li, B.; Lu, G.; Ma, J. Enhancing catalytic activity and stability for CO<sub>2</sub> methanation on Ni@MOF-5 via control of active species dispersion. *Chem. Commun.* **2015**, *51*, 1728–1731. [[CrossRef](#)]

49. Rungtaweivoranit, B.; Baek, J.; Araujo, J.R.; Archanjo, B.S.; Yaghi, O.M.; Somorjai, G.A. Copper Nanocrystals Encapsulated in Zr-based Metal-Organic Frameworks for Highly Selective CO<sub>2</sub> Hydrogenation to Methanol. *Nano Lett.* **2016**, *16*, 7645–7649. [[CrossRef](#)]
50. An, B.; Zhang, J.; Cheng, K.; Ji, P.; Wang, C.; Lin, W. Confinement of Ultrasmall Cu/ZnOx Nanoparticles in Metal-Organic Frameworks for Selective Methanol Synthesis from Catalytic Hydrogenation of CO<sub>2</sub>. *J. Am. Chem. Soc.* **2017**, *139*, 3834–3840. [[CrossRef](#)]
51. Liu, J.; Zhang, A.; Liu, M.; Hu, S.; Ding, F.; Song, C.; Guo, X. Fe-MOF-derived highly active catalysts for carbon dioxide hydrogenation to valuable hydrocarbons. *J. CO<sub>2</sub> Util.* **2017**, *21*, 100–107. [[CrossRef](#)]
52. Wang, Y.; Kazumi, S.; Gao, W.; Gao, X.; Li, H.; Guo, X.; Yoneyama, Y.; Yang, G.; Tsubaki, N. Direct conversion of CO<sub>2</sub> to aromatics with high yield via a modified Fischer-Tropsch synthesis pathway. *Appl. Catal. B Env.* **2020**, *269*, 118792–118801. [[CrossRef](#)]
53. Martín, N.; Portillo, A.; Ateka, A.; Cirujano, F.G.; Oar-Arteta, L.; Aguayo, A.T.; Dusselier, M. MOF-derived/zeolite hybrid catalyst for the production of light olefins from CO<sub>2</sub>. *ChemCatChem* **2020**, *12*, 5750–5758. [[CrossRef](#)]
54. Ramirez, A.; Gevers, L.; Bavykina, A.; Ould-Chikh, S.; Gascon, J. Metal Organic Framework-Derived Iron Catalysts for the Direct Hydrogenation of CO<sub>2</sub> to Short Chain Olefins. *ACS Catal.* **2018**, *8*, 9174–9182. [[CrossRef](#)]
55. Chen, C.S.; Cheng, W.H.; Lin, S. Mechanism of CO formation in reverse water-gas shift reaction over Cu/Al<sub>2</sub>O<sub>3</sub> catalyst. *Catal. Lett.* **2000**, *68*, 45–48. [[CrossRef](#)]
56. Porosoff, M.D.; Baldwin, J.; Peng, X.; Mpourmpakis, G.; Willauer, H.D. Potassium Promoted Molybdenum Carbide as a Highly Active and Selective Catalyst for CO<sub>2</sub> Conversion to CO. *ChemSusChem* **2017**, *10*, 2408–2415. [[CrossRef](#)] [[PubMed](#)]
57. Matsubu, J.C.; Yang, V.N.; Christopher, P. Isolated Metal Active Site Concentration and Stability Control Catalytic CO<sub>2</sub> Reduction Selectivity. *J. Am. Chem. Soc.* **2015**, *137*, 3076–3084. [[CrossRef](#)] [[PubMed](#)]
58. Kim, S.S.; Lee, H.H.; Hong, S.C. A study on the effect of support's reducibility on the reverse water-gas shift reaction over Pt catalysts. *Appl. Catal. A* **2012**, *423*, 100–107. [[CrossRef](#)]
59. Lu, B.; Kawamoto, K. Preparation of mesoporous CeO<sub>2</sub> and monodispersed NiO particles in CeO<sub>2</sub>, and enhanced selectivity of NiO/CeO<sub>2</sub> for reverse water gas shift reaction. *Mater. Res. Bull.* **2014**, *53*, 70–78. [[CrossRef](#)]
60. Loiland, J.A.; Wulfers, M.J.; Marinkovic, N.S.; Lobo, R.F. Fe/γ-Al<sub>2</sub>O<sub>3</sub> and Fe-K/γ-Al<sub>2</sub>O<sub>3</sub> as reverse water-gas shift catalysts. *Catal. Sci. Technol.* **2016**, *6*, 5267. [[CrossRef](#)]
61. Pour, A.N.; Shahri, S.M.K.; Bozorgzadeh, H.R.; Zamani, Y.; Tavasoli, A.; Marvast, M.A. Effect of Mg, La and Ca promoters on the structure and catalytic behavior of iron-based catalysts in Fischer-Tropsch synthesis. *Appl. Catal. A* **2008**, *348*, 201–208. [[CrossRef](#)]
62. Li, J.; Cheng, X.; Zhang, C.; Wang, J.; Dong, W.; Yang, Y.; Li, Y. Alkalis in iron-based Fischer-Tropsch synthesis catalysts; distribution, migration and promotion. *J. Chem. Technol. Biotechnol.* **2017**, *92*, 1472–1480. [[CrossRef](#)]
63. Dorner, R.W.; Hardy, D.R.; Williams, F.W.; Willauer, H.D. K and Mn doped iron-based CO<sub>2</sub> hydrogenation catalysts; Detection of KAlH<sub>4</sub> as part of the catalyst's active phase. *Appl. Catal. A* **2010**, *373*, 112–121. [[CrossRef](#)]
64. Rodemerck, U.; Holenā, M.; Wagner, E.; Smejkal, Q.; Barkschat, A.; Baerns, M. Catalyst Development for CO<sub>2</sub> Hydrogenation to Fuels. *ChemCatChem* **2013**, *5*, 1948–1955. [[CrossRef](#)]
65. Numpilai, T.; Witoon, T.; Chanlek, N.; Limphirat, W.; Bonura, G.; Chareonpanich, M.; Limtrakul, L. Structure-activity relationships of Fe-Co/K-Al<sub>2</sub>O<sub>3</sub> catalysts calcined at different temperatures for CO<sub>2</sub> hydrogenation to light olefins. *Appl. Catal. A* **2017**, *547*, 219–229. [[CrossRef](#)]
66. Zhao, T.; Hui, Y.; Li, Z. Controllable preparation of ZIF-67 derived catalyst for CO<sub>2</sub> methanation. *Mol. Catal.* **2019**, *474*, 110421–110430. [[CrossRef](#)]
67. Lin, X.; Wang, S.; Tu, W.; Hu, Z.; Ding, Z.; Hou, Y.; Xu, R.; Dai, W. MOF-derived hierarchical hollow spheres composed of carbon-confined Ni nanoparticles for efficient CO<sub>2</sub> methanation. *Catal. Sci. Technol.* **2019**, *9*, 731–738. [[CrossRef](#)]
68. Fang, R.; Chen, L.; Shen, Z.; Li, Y. Efficient hydrogenation of furfural to fufuryl alcohol over hierarchical MOF immobilized metal catalysts. *Catal. Today* **2021**, *368*, 217–223. [[CrossRef](#)]
69. Song, Y.; Feng, X.; Chen, J.S.; Brzezinski, C.; Xu, Z.; Lin, W. Multistep Engineering of Synergistic Catalysts in a Metal-Organic Framework for Tandem C-O Bond Cleavage. *J. Am. Chem. Soc.* **2020**, *142*, 4872–4882. [[CrossRef](#)]
70. Phan, D.P.; Lee, E.Y. Phosphoric acid enhancement in a Pt-encapsulated Metal-Organic Framework (MOF) bifunctional catalyst for efficient hydro-deoxygenation of oleic acid from biomass. *J. Catal.* **2020**, *386*, 19–29. [[CrossRef](#)]
71. Yuan, Q.; Zhang, D.; Van Haandel, L.; Ye, F.; Xue, T.; Hensen, E.J.M.; Guan, Y. Selective liquid phase hydrogenation of furfural to furfuryl alcohol by Ru/Zr-MOFs. *J. Mol. Catal. A Chem.* **2015**, *406*, 58–64. [[CrossRef](#)]
72. Fulajtárova, K.; Soták, T.; Hronec, M.; Vávra, I.; Dobročka, E.; Omastová, M. Aqueous phase hydrogenation of furfural to furfuryl alcohol over Pd-Cu catalysts. *Appl. Catal. A Gen.* **2015**, *502*, 78–85. [[CrossRef](#)]
73. Feng, J.; Li, M.; Zhong, Y.; Xu, Y.; Meng, X.; Zhao, Z.; Feng, C. Hydrogenation of levulinic acid to γ-valerolactone over Pd@UiO-66-NH<sub>2</sub> with high metal dispersion and excellent reusability. *Microporous Mesoporous Mater.* **2020**, *294*, 109858–109867. [[CrossRef](#)]
74. Aijaz, A.; Karkamkar, A.; Choi, Y.J.; Tsumori, N.; Rönnebro, E.; Autrey, T.H.; Shioyama, H.; Xu, Q. Immobilizing Highly Catalytically Active Pt Nanoparticles inside the Pores of Metal-Organic Framework. *J. Am. Chem. Soc.* **2012**, *134*, 13–16. [[CrossRef](#)] [[PubMed](#)]

75. Lin, S.; Kumar Reddy, D.H.; Bediako, J.K.; Song, M.H.; Wei, W.; Kim, J.A.; Yun, Y.S. Effective adsorption of Pd(II), Pt(IV) and Au(III) by Zr(IV)-based metal–organic frameworks from strongly acidic solutions. *J. Mater. Chem. A* **2017**, *5*, 13557–13564. [[CrossRef](#)]
76. Li, X.; Guo, Z.; Xiao, C.; Goh, T.W.; Tesfagaber, D.; Huang, W. Tandem catalysis by palladium nanoclusters encapsulated in metal–organic frameworks. *ACS Catal.* **2014**, *4*, 3490–3497. [[CrossRef](#)]
77. Klet, R.C.; Liu, Y.; Wang, T.C.; Hupp, J.T.; Farha, O.K. Evaluation of Brønsted acidity and proton topology in Zr- and Hf-based metal–organic frameworks using potentiometric acid–base titration. *J. Mater. Chem. A* **2016**, *4*, 1479–1485. [[CrossRef](#)]
78. Cirujano, F.G.; Corma, A.; Llabrés, I.; Xamena, F.X. Zirconium-containing metal organic frameworks as solid acid catalysts for the esterification of free fatty acids: Synthesis of biodiesel and other compounds of interest. *Catal. Today* **2015**, *257*, 213–220. [[CrossRef](#)]
79. Li, X.; Deng, Q.; Yu, L.; Gao, R.; Tong, Z.; Lu, C.; Wang, J.; Zeng, Z.; Zou, J.J.; Deng, S. Double-metal cyanide as an acid and hydrogenation catalyst for the highly selective ring-rearrangement of biomass-derived furfuryl alcohol to cyclopentenone compounds. *Green Chem.* **2020**, *22*, 2549–2557. [[CrossRef](#)]
80. Kim, D.W.; Kim, H.G.; Cho, D.H. Catalytic performance of MIL-100 (Fe, Cr) and MIL-101 (Fe, Cr) in the isomerization of endo- to exo-dicyclopentadiene. *Catal. Commun.* **2016**, *73*, 69–73. [[CrossRef](#)]
81. Rinaldi, R.; Schüth, F. Design of solid catalysts for the conversion of biomass. *Energy Environ. Sci.* **2009**, *2*, 610–626. [[CrossRef](#)]
82. Geilen, F.M.A.; Engendahl, B.; Harwardt, A.; Marquardt, W.; Klankermayer, J.; Leitner, W. Selective and flexible transformation of biomass-derived platform chemicals by a multifunctional catalytic system. *Angew. Chem. Int. Ed.* **2010**, *49*, 5510–5514. [[CrossRef](#)] [[PubMed](#)]
83. Zhang, D.; Ye, F.; Guan, Y.; Wang, Y.; Hensen, E.J.M. Hydrogenation of  $\gamma$ -valerolactone in ethanol over Pd nanoparticles supported on sulfonic acid functionalized MIL-101. *RSC Adv.* **2014**, *4*, 39558–39564. [[CrossRef](#)]
84. Valekar, A.H.; Lee, M.; Yoon, J.W.; Kwak, J.; Hong, D.Y.; Oh, K.R.; Cha, G.Y.; Kwon, Y.U.; Jung, J.; Chang, J.S.; et al. Catalytic Transfer Hydrogenation of Furfural to Furfuryl Alcohol under Mild Conditions over Zr-MOFs: Exploring the Role of Metal Node Coordination and Modification. *ACS Catal.* **2020**, *10*, 3720–3732. [[CrossRef](#)]
85. Bai, Y.; Dou, Y.; Xie, L.H.; Rutledge, W.; Li, J.R.; Zhou, H.C. Zr-based metal–organic frameworks: Design, synthesis, structure, and applications. *Chem. Soc. Rev.* **2016**, *45*, 2327–2367. [[CrossRef](#)] [[PubMed](#)]
86. Li, H.; He, J.; Riisager, A.; Saravanamurugan, S.; Song, B.; Yang, S. Acid–base bifunctional zirconium N-alkyltriphosphate nanohybrid for hydrogen transfer of biomass-derived carboxides. *ACS Catal.* **2016**, *6*, 7722–7727. [[CrossRef](#)]
87. Li, H.; Liu, X.; Yang, T.; Zhao, W.; Saravanamurugan, S.; Yang, S. Porous Zirconium–Furandicarboxylate Microspheres for Efficient Redox Conversion of Biofurans. *ChemSusChem* **2017**, *10*, 1761–1770. [[CrossRef](#)]
88. Yang, D.; Bernales, V.; Islamoglu, T.; Farha, O.K.; Hupp, J.T.; Cramer, C.J.; Gagliardi, L.; Gates, B.C. Tuning the Surface Chemistry of Metal Organic Framework Nodes: Proton Topology of the Metal-Oxide-Like Zr<sub>6</sub> Nodes of UiO-66 and NU-1000. *J. Am. Chem. Soc.* **2016**, *138*, 15189–15196. [[CrossRef](#)]
89. Yang, D.; Gaggioli, C.A.; Ray, D.; Babucci, M.; Gagliardi, L.; Gates, B.C. Tuning Catalytic Sites on Zr<sub>6</sub>O<sub>8</sub> Metal–Organic Framework Nodes via Ligand and Defect Chemistry Probed with tert-Butyl Alcohol Dehydration to Isobutylene. *J. Am. Chem. Soc.* **2020**, *142*, 8044–8056. [[CrossRef](#)]
90. Jung, K.D.; Bell, A.T. Role of Hydrogen Spillover in Methanol Synthesis over Cu/ZrO<sub>2</sub>. *J. Catal.* **2000**, *193*, 207–223. [[CrossRef](#)]
91. Li, D.; Xu, H.Q.; Jiao, L.; Jiang, H.L. Metal-organic frameworks for catalysis: State of the art, challenges, and opportunities. *EnergyChem* **2019**, *1*, 100005. [[CrossRef](#)]
92. Han, A.; Wang, B.; Kumar, A.; Qin, Y.; Jin, J.; Wang, X.; Yang, C.; Dong, B.; Jia, Y.; Liu, J.; et al. Recent Advances for MOF-Derived Carbon-Supported Single-Atom Catalysts. *Small Methods* **2019**, *3*, 1800471–1800492. [[CrossRef](#)]
93. Salunkhe, R.R.; Kaneti, Y.V.; Kim, J.; Kim, J.H.; Yamauchi, Y. Nanoarchitectures for Metal–Organic Framework-Derived Nanoporous Carbons toward Supercapacitor Applications. *Acc. Chem. Res.* **2016**, *49*, 2796–2806. [[CrossRef](#)] [[PubMed](#)]
94. Wang, Q.; Astruc, D. State of the Art and Prospects in Metal–Organic Framework (MOF)-Based and MOF-Derived Nanocatalysis. *Chem. Rev.* **2020**, *120*, 1438–1511. [[CrossRef](#)] [[PubMed](#)]
95. Yang, S.; Peng, L.; Bulut, S.; Queen, W.L. Recent Advances of MOFs and MOF-Derived Materials in Thermally Driven Organic Transformations. *Chem. Eur. J.* **2019**, *25*, 2161–2178. [[CrossRef](#)]
96. Chaikittisilp, W.; Hu, M.; Wang, H.; Huang, H.S.; Fujita, T.; Wu, K.C.W.; Chen, L.C.; Yamauchi, Y.; Ariga, K. Nanoporous carbons through direct carbonization of a zeolitic imidazolate framework for supercapacitor electrodes. *Chem. Commun.* **2012**, *48*, 7259–7261. [[CrossRef](#)]
97. Fang, R.; Dhakshinamoorthy, A.; Li, Y.; Garcia, H. Metal organic frameworks for biomass conversion. *Chem. Soc. Rev.* **2020**, *49*, 3638–3687. [[CrossRef](#)]
98. Liao, Y.; Van Chi, N.; Ishiguro, N.; Young, A.P.; Tsung, C.; Wu, K.C. Environmental Engineering a homogeneous alloy-oxide interface derived from metal-organic frameworks for selective oxidation of 5-hydroxymethylfurfural to 2, 5-furandicarboxylic acid. *Applied Catalysis B* **2020**, *270*, 118805–118817. [[CrossRef](#)]
99. Liao, Y.; Chen, J.E.; Isida, Y.; Yonezawa, T.; Chang, W. De Novo Synthesis of Gold-Nanoparticle-Embedded, Nitrogen-Doped Nanoporous Carbon Nanoparticles (Au@NC) with Enhanced Reduction Ability. *ChemCatChem* **2016**, *44*, 502–509. [[CrossRef](#)]

100. Liao, Y.; Huang, Y.; Chen, H.M.; Komaguchi, K.; Hou, H.; Henzie, J.; Yamauchi, Y.; Ide, Y.; Wu, K.C.; Liao, Y.; et al. Mesoporous TiO<sub>2</sub> Embedded with a Uniform Distribution of CuO Exhibit Enhanced Charge Separation and Photocatalytic Efficiency. *ACS Appl. Mater. Interfaces* **2017**, *9*, 42425–42429. [[CrossRef](#)]
101. Abad, A.; Concepción, P.; Corma, A. A Collaborative Effect between Gold and a Support Induces the Selective Oxidation of Alcohols. *Angew. Chem. Int. Ed.* **2005**, *44*, 4066–4069. [[CrossRef](#)]
102. Kim, B.Y.; Shim, I.B.; Araci, Z.O.; Scott Saavedra, S.; Monti, O.L.A.; Armstrong, N.R.; Sahoo, R.; Srivastava, D.N.; Pyun, J. Synthesis and colloidal polymerization of ferromagnetic Au-Co nanoparticles into Au-Co<sub>3</sub>O<sub>4</sub> nanowires. *J. Am. Chem. Soc.* **2010**, *132*, 3234–3235. [[CrossRef](#)] [[PubMed](#)]
103. Wu, Z.; Deng, J.; Liu, Y.; Xie, S.; Jiang, Y.; Zhao, X.; Yang, J.; Arandiyán, H.; Guo, G.; Dai, H. Three-dimensionally ordered mesoporous Co<sub>3</sub>O<sub>4</sub>-supported Au—Pd alloy nanoparticles: High-performance catalysts for methane combustion. *J. Catal.* **2015**, *332*, 13–24. [[CrossRef](#)]
104. Casanova, O.; Iborra, S.; Corma, A. Biomass into Chemicals: Aerobic Oxidation of 5-Hydroxy-methyl-2-furfural into 2, 5-Furandicarboxylic Acid with Gold Nanoparticle Catalysts. *ChemSusChem* **2009**, *2*, 1138–1144. [[CrossRef](#)] [[PubMed](#)]
105. Ardemani, L.; Cibirin, G.; Dent, A.J.; Isaacs, M.A.; Kyriakou, G.; Lee, A.F.; Parlett, C.M.A.; Parry, S.A.; Wilson, K. Solid base catalysed 5-HMF oxidation to 2,5-FDCA over Au/hydrotalcites: Fact or fiction? *Chem. Sci.* **2015**, *6*, 4940–4945. [[CrossRef](#)]
106. Van Nguyen, C.; Liao, Y.T.; Kang, T.C.; Chen, J.E.; Yoshikawa, T.; Nakasaka, Y.; Masuda, T.; Wu, K.C.W. A Metal-Free, High Nitrogen-Doped Nanoporous Graphitic Carbon Catalyst for an Effective Aerobic HMF-to-FDCA Conversion. *Green Chem.* **2016**, *18*, 5957–5961. [[CrossRef](#)]
107. Zhou, C.; Deng, W.; Wan, X.; Zhang, Q.; Yang, Y. Functionalized Carbon Nanotubes for Biomass Conversion: The Base-Free Aerobic Oxidation of 5-Hydroxymethyl- furfural to 2,5-Furandicarboxylic Acid over Platinum Supported on a Carbon Nanotube Catalyst. *ChemCatChem* **2015**, *7*, 2853–2863. [[CrossRef](#)]
108. Feng, Y.; Jia, W.; Yan, G.; Zeng, X.; Sperry, J.; Xu, B.; Sun, Y.; Tang, X.; Lei, T.; Lin, L. Insights into the active sites and catalytic mechanism of oxidative esterification of 5-hydroxymethylfurfural by metal–organic frameworks-derived N-doped carbon. *J. Catal.* **2020**, *381*, 570–578. [[CrossRef](#)]
109. Zhang, M.; Townend, I.; Cai, H.; He, J.; Mei, X. The influence of seasonal climate on the morphology of the mouth-bar in the Yangtze Estuary, China. *Cont. Shelf Res.* **2018**, *153*, 30–49. [[CrossRef](#)]
110. Zhong, W.; Liu, H.; Bai, C.; Liao, S.; Li, Y. Base-free oxidation of alcohols to esters at room temperature and atmospheric conditions using nanoscale Co-based catalysts. *ACS Catal.* **2015**, *5*, 1850–1856. [[CrossRef](#)]
111. Wu, G.; More, K.L.; Johnston, C.M.; Zelenay, P. High-performance electrocatalysts for oxygen reduction derived from polyaniline, iron, and cobalt. *Science* **2011**, *332*, 443–447. [[CrossRef](#)] [[PubMed](#)]
112. Deng, D.; Yu, L.; Chen, X.; Wang, G.; Jin, L.; Pan, X.; Deng, J.; Sun, G.; Bao, X. Iron Encapsulated within Pod-like Carbon Nanotubes for Oxygen Reduction Reaction. *Angew. Chem. Int. Ed.* **2013**, *52*, 371–375. [[CrossRef](#)]
113. Bao, L.; Sun, F.; Zhang, G.; Hu, T.L. High-efficient Aerobic Oxidation of Biomass-derived 5-Hydroxymethylfurfural to 2,5-Furandicarboxylic Acid over Holey 2D Mn<sub>2</sub>O<sub>3</sub> Nanoflakes from a Mn-based MOF. *ChemSusChem* **2019**, *13*, 548–555. [[CrossRef](#)]
114. Fang, R.; Tian, P.; Yang, X.; Luque, R.; Li, Y. Encapsulation of ultra fine metal-oxide nanoparticles within mesopores for biomass-derived catalytic applications. *Chem. Sci.* **2018**, *9*, 1854–1859. [[CrossRef](#)]
115. Meng, J.; Niu, C.; Xu, L.; Li, J.; Liu, X.; Wang, X.; Wu, Y.; Xu, X.; Chen, W.; Li, Q.; et al. General Oriented Formation of Carbon Nanotubes from Metal–Organic Frameworks. *J. Am. Chem. Soc.* **2017**, *139*, 8212–8221. [[CrossRef](#)]
116. Fang, R.; Luque, R.; Li, Y. Selective aerobic oxidation of biomass-derived HMF to 2,5-diformylfuran using a MOF-derived magnetic hollow Fe–Co nanocatalyst. *Green Chem.* **2016**, *18*, 3152–3157. [[CrossRef](#)]